A Review of the Recent Developments in Laminar, Transitional, Quasi-turbulent and Turbulent Forced and Mixed Convective Flow through Horizontal Tubes

Josua P. Meyer and Marilize Everts
University of Pretoria, South Africa

Abstract

The laminar and turbulent flow regimes have been extensively investigated from as early as 1883, and research has been devoted to the transitional flow regime since the 1990s. However, there are several gaps in the mixed convection literature, especially when the flow is still developing. The purpose of this chapter is to combine fragmented previous work of the authors to create a new coherent body of work with new perspectives. Specifically, focussing on the heat transfer and pressure drop characteristics of developing and fully developed flow in smooth horizontal tubes for forced and mixed convection conditions. The flow regimes that were covered were laminar (forced and mixed convection), transitional (forced and mixed convection), quasi-turbulent and turbulent.

Keywords: laminar, transitional, quasi-turbulent, turbulent, forced convection, mixed convection, tubes, developing flow, fully developed flow.

1. Introduction

The state of flow (laminar, transition, quasi-turbulent, or turbulent) can affect the performance of many thermal systems. Heat exchanger performance is a classic example. Heat exchangers have a wide range of domestic and industrial applications, especially in the generation and consumption of electrical energy. On the generation side, heat exchangers are indispensable components in the cycles of fossil fuel, nuclear and solar power plants. They are used to transfer heat in boilers from the energy source (fossils, nuclear reaction, solar, etc.) to the fluids (usually steam) used to drive turbines that generate electricity. Downstream of turbines, heat exchangers are used to condense steam and reject heat to the environment. On the consumption side, heat exchangers are found in the process, petrochemical, petroleum, transport, sewage treatment, manufacturing and heating, ventilation and air-conditioning industries. The efficiency of generating energy and using energy directly depends on the effectiveness of heat exchangers.

The state of flow can also affect the performance of systems that experience significant entrance effects. For fluid flow in a tube with heat transfer, the thermal entrance length measured from a tube inlet is a very important aspect for design engineers. The reason is that it determines whether the heat transfer coefficients are dependent on (developing flow) or independent of (fully developed flow) axial tube position. When high Prandtl number fluids such as oils are used, the thermal entrance length can become very long, especially at high laminar Reynolds numbers (close to the transitional flow regime). Extensive research has been done on the thermal entrance length in the laminar flow regime; however, there are still some gaps in the mixed convection literature. Although free convection effects have been found to decrease the thermal entrance length, there is not only uncertainty regarding the correlation for calculating the thermal entrance length, but also the definition of the point of fully developed flow in mixed convection heat transfer.

Much attention has also been paid to mixed convection laminar heat transfer in horizontal circular tubes with a constant heat flux boundary condition, especially when the flow is fully developed. While laminar heat transfer correlations are readily available in heat transfer textbooks, these equations and graphs are usually based on analytical solutions to the governing equations for laminar flow. The information is therefore restricted to constant fluid property situations, an assumption that is not valid in actual practice. Furthermore, the differing behaviour of the local heat transfer characteristics of different Prandtl number fluids makes it challenging to obtain a single correlation.

Cheng and Ou [1] found that for Rayleigh numbers less than 3.75×10^5, the local Nusselt numbers did not decrease asymptotically and became constant. The Nusselt numbers decreased near the inlet of the test section, and then increased along the tube length before it became constant. Although three regions were observed for the behaviour of the local laminar Nusselt numbers for mixed convection conditions, the boundaries between the three regions and the heat transfer characteristics in each region were not defined qualitatively and quantitatively.

For transitional flow, Ghajar and co-workers [2-18] broke new ground with investigating the effect of inlet geometry and heating on transition, making it possible for others, such as Meyer and co-workers [19-43], to follow. However, the focus of previous studies was not on the characteristics of developing flow, but rather on the effect of different inlet geometries, enhanced tubes, micro-channels, multiple circular tubes, annular flow and different Prandtl number fluids. In general, it was found that transition was delayed for smoother inlet geometries, as well as increasing heat fluxes, but occurred earlier with increasing surface roughness, helix angle in enhanced tubes, or decreasing twist ratio when twisted tape inserts were used. Therefore, the Reynolds number range in which transition occurred could be manipulated by changing the inlet geometry, heat flux or tube surface. Recent advances in transitional flow investigations have been made by Abraham and co-workers [44-48]. A computational model was developed that was able to produce accurate heat transfer and pressure drop results for transitional flow, as well as laminar and turbulent flows in circular tubes and nonround duct shapes. Heat transfer and pressure drop correlations were also presented, however, it should be noted that the model and correlations were limited to forced convection conditions only. In this chapter, a clear distinction was made between forced and mixed convection.

Until recently, no experimental studies have been specifically devoted to the heat transfer characteristics of developing flow in the transitional flow regime, how they change along the tube length, how they differ from that of fully developed flow, and how they are affected by free convection effects. Furthermore, the methods that are used to identify the boundaries of the transitional flow regime not only rely on subjective decisions, but also do not distinguish between the transitional and quasi-turbulent flow regimes. An understanding of the factors that influence the start and end of the transitional flow regime, as well as an understanding of the heat transfer and pressure drop behaviour in this regime is required in order to select or develop appropriate heat transfer and pressure drop correlations for transitional flow. As this flow regime has not yet been properly understood and limited experimental data are available [49], the available correlations to predict the heat transfer coefficients and friction factors are still very limited [9]. The existing correlations are restricted to forced convection conditions, specific inlet geometries or high Prandtl number fluids and no clear distinction has been made between the transitional and quasi-turbulent flow regimes.

Furthermore, although heat transfer and pressure drop are usually investigated independently, a direct relationship exists, which is often overlooked [50]. This relationship has been investigated in the laminar and turbulent flow regimes, and correlations have been developed to quantify these relationships [51-54]. However, no correlations have been developed to quantitatively describe the relationship between heat transfer and pressure drop in the transitional flow regime. It is important to investigate this relationship, especially in the transitional flow regime, because there is a fundamental gap in the literature on this subject field. This will be the first step before similar relationships can be developed for more complex geometries. Specifically, for complex geometries, it will be much easier for engineers to obtain either the heat transfer coefficients or pressure drops, because this will save time and money. This relationship will enable them to calculate either the heat transfer coefficients or the friction factors when the other variable is unavailable. Furthermore, it will also give additional insight into the trade-off between high heat transfer coefficients and low pressure drops during the design process.

As the densities of fluids are dependent on temperature, the addition of heat to the tube wall causes temperature gradients inside the thermal boundary layer that lead to density differences and buoyancy effects in the presence of gravity [55]. Free convection effects not only increase the heat transfer and pressure drop, but also reduce the thermal entrance length and induce an early transition to turbulent flow [56]. When selecting appropriate equations, a flow regime map is a valuable tool that can be used to determine whether free convection effects can be neglected (forced convection dominates) or whether it is significant (mixed convection dominates).

Although Tam *et al*. [11] developed a versatile flow regime map that accounts for different inlet geometries in horizonal tubes with a constant heat flux boundary condition, this map was developed using experimental data [6] obtained in relatively large diameter tubes and high Prandtl number fluids, especially in the laminar flow regime . Therefore, although the existing flow regime map may be very accurate for high Prandtl number fluids, it may become inaccurate once the Prandtl number and tube diameter are decreased, for example, when water is used in small diameter tubes. The result is that the flow is predicted to be in the forced convection regions, while free convection effects are significant and the flow is actually dominated by mixed convection. Furthermore, the existing flow regime maps were also developed for fully developed flow, while the majority of the flow in heat exchangers might still be developing, especially at high Reynolds numbers close to the transitional flow regime.

Overall, it can be concluded that there are several gaps in the mixed convection literature, especially when the flow is still developing. Thermal entrance length, heat transfer, and pressure drop correlations that are valid for both developing and fully developed laminar and transitional flow in mixed convection conditions, are required, as well as a flow regime map that accounts for low Prandtl number fluids and for developing flow. This will not only enable designers to optimise the design of heat exchangers, but also improve the fundamental understanding of mixed convection developing and fully developed flow.

The purpose of this chapter is to combine fragmented previous work [22, 24-26, 31, 32] of the authors to create a new coherent body of work with new perspectives. Specifically, focussing on the heat transfer and pressure drop characteristics of developing and fully developed flow of low Prandtl number fluids in smooth horizontal tubes for forced and mixed convection conditions. The flow

regimes that were covered were laminar (forced and mixed convection), transitional (forced and mixed convection), quasi-turbulent and turbulent. In general a constant heat flux (uniform wall heating) boundary condition was used, except for the work in the turbulent flow regime [32] where both a constant heat flux and a constant surface temperature boundary condition were used.

2. Flow Regime Nomenclature

Although the Reynolds number boundaries between the laminar and transitional flow regimes have been described in literature, the descriptions are in general qualitative and relied on visual observations, which were subjective. Furthermore, in most of these cases, no clear distinction between the transitional and quasi-turbulent flow regimes was made. When large databases are collected, it is challenging to objectively and consistently identify the different boundaries. The result is that different transition outcomes can be generated by different people from the same data. Therefore, to be able to quantitatively investigate transitional flow and compare the results of different studies, Everts and Meyer [24] quantified the boundaries between the flow regimes and developed terminology to define transitional flow characteristics. To aid in the discussion of nomencaluture of the different flow regimes, Fig. 1 has been prepared. That figure identifies the flow regimes for various hydrodynamic and thermal parameters.

Fig. 1 is a schematic representation of the flow regimes in terms of the Nusselt numbers (Fig. 1(a)), Colburn *j*-factors (Fig. 1(b)) and friction factors (Fig. 1(c)) as a function of Reynolds number. The boundaries of the different flow regimes (Re_{cr}, Re_{qt} and Re_t) are indicated on the *x*-axis. The gradients of the Nusselt number (*dNu*/*dRe*), Colburn *j*-factor (*dj*/*dRe*) and friction factor (*df*/*dRe*) lines in the different flow regimes are defined along the *L*-*L*, *TG*-*TG*, *QT*-*QT* and *T*-*T* lines.

The boundaries of the transitional flow regime (Re_{cr} and Re_{qt}) could be identified from the standard deviation of the temperature and mass flow rate measurements [24]. However, this method cannot be used to identify the start of the turbulent flow regime, Re_t, because there is no significant difference between the standard deviations of the mass flow rate and temperature measurements in the quasi-turbulent and turbulent flow regimes [28]. The Nusselt numbers and Colburn *j*-factors were used to define the boundaries of the different flow regimes because these parameters are generally available (when the experimental data of other studies are analysed and investigated), while the temperature and mass flow rate measurements are not necessarily available. The results in terms of the Nusselt number and Colburn *j*-factor lines were used complementary; it was found that some boundaries were easier to identify using the Nusselt number lines, and others using the Colburn *j*-factor lines. Furthermore, as will be shown later (in Fig. 12), the flow regime boundaries are the same for the pressure drop and heat transfer results. Therefore, the boundaries identified using the Nusselt number and Colburn *j*-factor results are also valid for the friction factor results.

2.1. Flow regime boundaries

2.1.1. Start of the transitional flow regime, Re_{cr}

The start of the transitional flow regime (and end of the laminar flow regime), Re_{cr}, will be defined similarly to Ghajar and Tam [6] as:

$$Re = Re_{cr} \text{ when: } \left(\frac{dj}{dRe}\right)_{i-2:i} = 0 \quad (1)$$

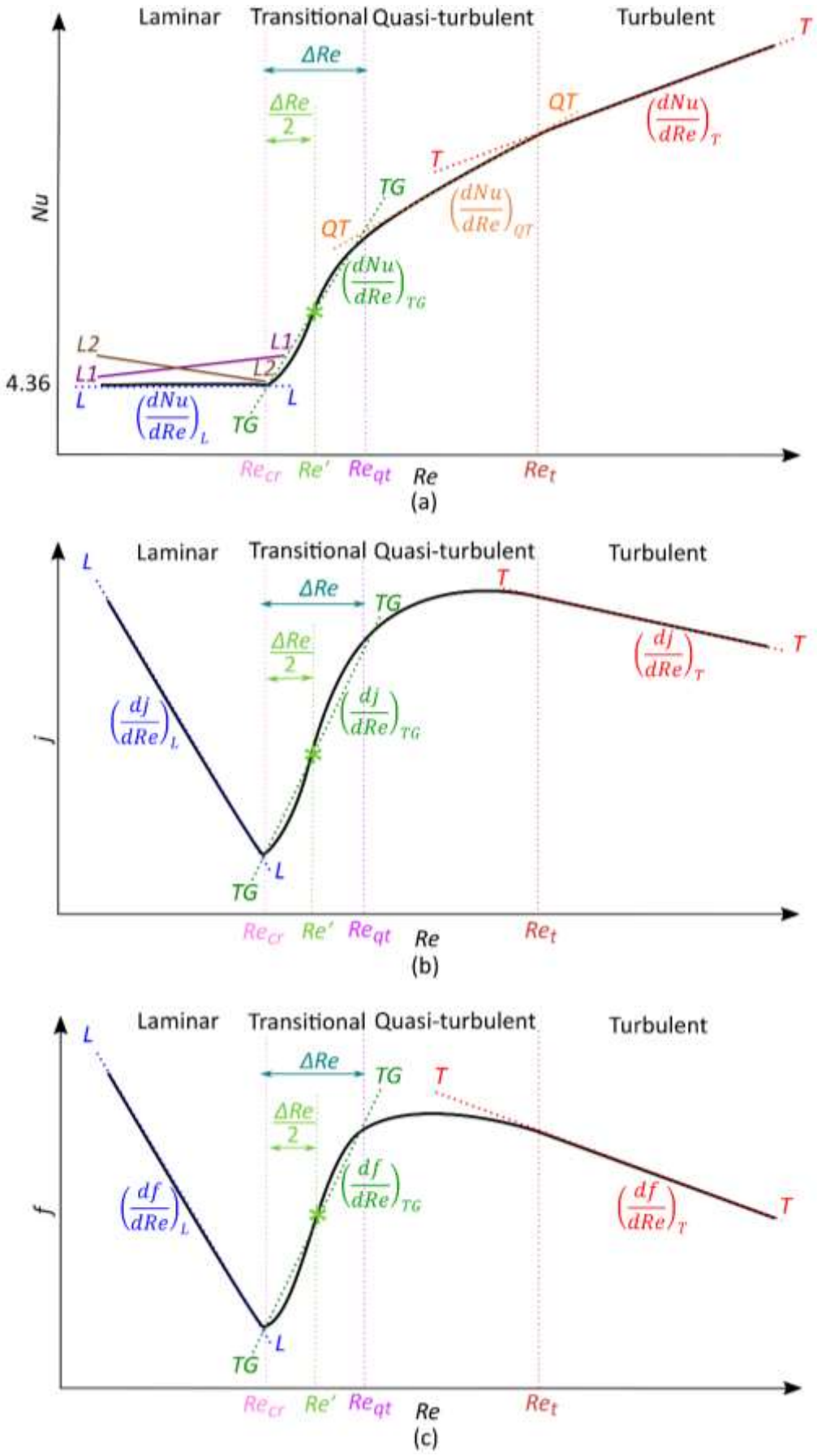

Fig. 1: Schematic representation of the different flow regimes in terms of (a) Nusselt number, (b) Colburn *j*-factor and (c) friction factor as a function of Reynolds number [24].

The notation *i*-2:*i* indicates that at an arbitrary location *i*, the gradient was obtained using the three data points at *Re*(*i*-2), *Re*(*i*-1) and *Re*(*i*), for increasing Reynolds numbers.

2.1.2. Start of the quasi-turbulent flow regime, Re_{qt}

The end of transition (Re_{qt}), which is also the start of the quasi-turbulent flow regime, is not as clear and easy to identify as the start of transition. This challenge has implications for accurately identifying the start of the turbulent flow regime (Re_t in Section 2.1.3). This possibly explains why, in literature, the quasi-turbulent flow regime is often regarded as part of either the transitional or turbulent flow regimes. However, Everts [57] found that the flow characteristics and heat transfer coefficients in the quasi-turbulent flow regime are unique and not exactly the same as the transitional or turbulent flow regimes. The flow characteristics are similar to turbulent flow because there is a negligible difference between the standard deviation of the temperature measurements in the quasi-turbulent and turbulent flow regimes [28]. However, the heat transfer coefficients in the quasi-turbulent flow regime are overpredicted by turbulent heat transfer correlations. Because the flow is not fully turbulent yet, this flow regime was named quasi-turbulent. The start of the quasi-turbulent flow regime is defined as:

$$Re = Re_{qt} \text{ when: } \left(\frac{d^2Nu}{dRe^2}\right)_{i:i+2} \geq -0.00015 \quad (2)$$

The notation *i*:*i*+2 indicates that at an arbitrary location *i*, the gradient is obtained using three data points at *Re*(*i*), *Re*(*i*+1) and *Re*(*i*+2) for increasing Reynolds numbers (while Eq. (1) used the results at the previous two Reynolds numbers).

2.1.3. Start of the turbulent flow regime, Re_t

The flow is considered fully turbulent once the Nusselt number and Colburn *j*-factor lines fall onto or become parallel to the heat transfer coefficients predicted by fully turbulent correlations, for example, the Colburn equation [51]. The start of the turbulent flow regime (and end of quasi-turbulent flow regime), Re_t, is defined as the Reynolds number at the intersection of the trendlines through the Nusselt number gradients in the quasi-turbulent ($(dNu/dRe)_{QT}$) and the turbulent ($(dNu/dRe)_T$) flow regimes:

$$Re = Re_t \text{ when: } \left(\frac{dNu}{dRe}\right)_{QT} = \left(\frac{dNu}{dRe}\right)_T \quad (3)$$

where

$$\left(\frac{dNu}{dRe}\right)_{QT} = 0.7054Re^{-0.534} \quad (4)$$

$$\left(\frac{dNu}{dRe}\right)_T = 0.0352Re^{-0.2} \quad (5)$$

Everts and Meyer [24] obtained Eq. (4) using power curves as fits through the Nusselt number gradients (of the experimental data obtained in different test sections at different axial positions and heat fluxes) in the quasi-turbulent flow regime ($Re_{cr} < Re < 6\,000$). Equation (5) was obtained by taking the derivative of the Colburn equation [51] (which is valid for fully turbulent flow) with respect to Reynolds number. However, an uncertainty of 10% was used due to the relatively high uncertainties (because of the small temperature differences) in the turbulent flow regime. Because a single trend line (Eq. (4)) was obtained through all the data in the quasi-turbulent flow regime, this value was true

for all the results. However, Everts and Meyer [24] noted this can be refined with experimental data (with low uncertainties, especially in the quasi-turbulent and turbulent flow regimes) by obtaining individual trendlines through data in the quasi-turbulent flow regime.

2.2. Flow characteristics

2.2.1. Laminar flow regime

It will be shown later (in Fig. 3(a)), local laminar Nusselt numbers can be divided into three regions: forced convection developing (FCD), mixed convection developing (MCD) and fully developed (FD). The trend of the Nusselt numbers as a function of Reynolds number is significantly affected by the heat transfer characteristics of these three regions.

2.2.1.1. Forced convection developing (FCD)

When the flow is still developing, the local Nusselt numbers decrease along the tube length, as the thermal boundary layer develops (entrance effects). As the thermal boundary layer thickness is very thin in this region, free convection effects are negligible. The thermal entrance length increases with increasing Reynolds number, therefore at a fixed axial position, the thermal boundary layer thickness decreases and the Nusselt numbers increase with increases in Reynolds number. The Nusselt numbers therefore form a diagonal line with a positive gradient (line *L*1-*L*1 in Fig. 1) and

$$\frac{dNu}{dRe} > 0 \tag{6}$$

2.2.1.2. Mixed convection developing (MCD)

In this region, the thermal boundary layer thickness is sufficient for free convection effects to be significant. As the flow is still developing, the thermal boundary layer thickness increases along the tube length. Free convection effects decrease the thermal entrance length [31], therefore at a fixed axial position, the thermal boundary layer thickness increases and the Nusselt number decreases (entrance effects) with increasing Reynolds number. It should however be noted that free convection effects increase with increasing thermal boundary layer thickness, which may lead to increasing Nusselt numbers along the tube length (free convection effects).

When the decrease in Nusselt number (due to the shorter thermal entrance length) is greater than the increase due to free convection effects, entrance effects dominate and $(dNu/dRe)_L > 0$ (Eq. (6)). However, when free convection effects dominate the entrance effects, the Nusselt numbers decrease with increasing Reynolds number, because the thermal boundary layer thickness and free convection effects decrease (line *L*2-*L*2 in Fig. 1). Consequently,

$$\frac{dNu}{dRe} < 0 \tag{7}$$

2.2.1.3. Fully developed (FD)

For fully developed forced convection flow in a tube heated at a constant heat flux, the Nusselt numbers form a horizontal line in Fig. 1(a) and should be equal to 4.36. Therefore

$$\frac{dNu}{dRe} = 0 \tag{8}$$

When the flow is dominated by mixed convection, the Nusselt numbers should be greater than 4.36. The Nusselt numbers decrease with increasing Reynolds number, because the free convection effects decrease, therefore $(dNu/dRe)_L < 0$ (Eq. (7)).

2.2.2. Transitional flow regime

Previous work that has been done on flow in the transitional flow regime concludes that the transitional flow regime can be manipulated by changing the inlet geometry and heat flux, and that it varies when different locations on the test section are considered. In order to quantify these changes in the transitional flow regime, the width of the transitional flow regime, ΔRe, and the transition gradients, TG_f and TG_j, are defined.

2.2.2.1. Width of the transitional flow regime

The width of the transitional flow regime represents the Reynolds number range in which transition occurs. It is defined as

$$\Delta Re = Re_{qt} - Re_{cr} \tag{9}$$

2.2.2.2. Transition gradient

The transition gradient, TG_j (indicated by the dotted green *TG-TG* line in Fig. 1(b)), represents the straight line between the Colburn *j*-factors at the start (Re_{cr}) and end (Re_{qt}) of the transitional flow regime. It can be calculated from

$$TG_j = \frac{j_{qt} - j_{cr}}{Re_{qt} - Re_{cr}} \tag{10}$$

Similarly, the transition gradient for friction factors represents the straight line between the friction factors at the start (Re_{cr}) and end (Re_{qt}) of the transitional flow regime:

$$TG_f = \frac{f_{qt} - f_{cr}}{Re_{qt} - Re_{cr}} \tag{11}$$

The transition gradients give good indications of how the heat transfer and pressure drop characteristics change in the transitional flow regime.

2.2.2.3. Transitional flow inflection point, Re'

Everts and Meyer [24] observed that when dNu/dRe is plotted as a function of Reynolds number, dNu/dRe reaches a prominent maximum at Re', which is in the middle of the transitional flow regime. Furthermore, when d^2Nu/dRe^2 is plotted as a function of Reynolds number, it follows that in the transitional flow regime the d^2Nu/dRe^2 gradient first increases with increasing Reynolds number up to a maximum, then it decreases (to negative gradients) to a minimum, before it increases again. The inflection point is where d^2Nu/dRe^2 changes from a maximum to a minimum. The inflection point is also prominent in the pressure drop results, as well as in the relationship between pressure drop and heat transfer results.

As schematically indicated (and exaggerated) by the 's'-curve in Fig. 1, the gradient of the heat transfer coefficients and friction factors increases with increasing Reynolds number in the lower half of the transitional flow regime and then decreases in the upper half as the flow approaches the quasi-turbulent flow regime. The transitional flow inflection point is in the middle of the transitional flow regime where the change in the trend of the flow characteristics occurs

$$Re' = \frac{Re_{cr} + Re_{qt}}{2} = Re_{cr} + \frac{\Delta Re}{2} \quad (12)$$

The inflection point predicted using Eq. (12), is within 4% of the middle of the transitional flow regime (obtained using Eqs. (1) and (2)). Therefore, as Re_{cr} and Re' are simpler to obtain than Re_{qt}, Eq. (12) can also be used to obtain the start of the quasi-turbulent flow regime.

2.2.3. Quasi-turbulent flow regime

Not much research has been devoted to the heat transfer and pressure drop characteristics in this flow regime and it is often regarded as part of the transitional flow regime because the flow is not fully turbulent yet [46]. Although the heat transfer characteristics are closer to those of turbulent flow, an extension of the straight line (on a log-log scale) of the turbulent Nusselt numbers as a function of Reynolds number overpredicts the Nusselt numbers in this regime [27], therefore $(dNu/dRe)_{QT} > (dNu/dRe)_{T}$. The Nusselt numbers in the quasi-turbulent flow regime increase with increasing Reynolds number and form a diagonal line (Fig. 1(a)). However, the Colburn *j*-factors in this regime increase and then decrease slightly with increasing Reynolds number, forming a concave curve as the flow regime changes from transitional to fully turbulent (Fig. 1(b)).

2.2.4. Turbulent flow regime

The Colburn *j*-factor is proportional to the Nusselt number, but varies inversely with Reynolds number. Therefore, although the turbulent Nusselt numbers increase with increasing Reynolds number, the increase in Nusselt number is less than the increase in Reynolds number, which leads to decreasing Colburn *j*-factors in the turbulent flow regime.

3. Laminar Forced Convection Thermal Entrance Length

According to authoritative heat transfer textbooks [51, 58-61], the theoretical thermal entrance length for laminar flow can be determined as:

$$Lt_{FC} = CRePrD \quad (13)$$

where $C = 0.05$

However, when the flow is simultaneously thermally and hydrodynamically developing, Meyer and Everts [31] found that a longer thermal entrance length is required than when the flow is hydrodynamically fully developed at the inlet of the test section. To illustrate this, Fig. 2 compares local Nusselt numbers as a function of the inverse of the Graetz number for bulk Reynolds numbers between 1 000 and 2 000 at constant heat fluxes of 0.5 kW/m^2 (filled markers) and 1 kW/m^2 (empty markers) in a 4 mm test section. The correlations of Siegel *et al*. [62] for hydrodynamically fully developed and thermally developing flow, and of Shah and London [60] for simultaneously hydrodynamically and thermally developing flow, are indicated by the black and red lines, respectively. The theoretical Nusselt number of 4.36 for fully developed forced convection laminar flow with a constant heat flux boundary condition is indicated by the horizontal black dotted line,

while a 5% and 10% increase from this Nusselt number is indicated by the horizontal blue and red dotted lines, respectively.

Because the correlation of Siegel *et al*. [62] was developed for hydrodynamically fully developed flow, the flow developed faster and the predicted Nusselt numbers were lower than for the correlation of Shah and London [60]. Siegel *et al*. [62] considered the flow to be fully developed once the local Nusselt numbers were within 5% of the theoretical fully developed Nusselt number of 4.36 and reported that this should occur at $1/Gz \geq 0.0425$. However, Fig. 2 indicates that the correlation of Shah and London [60] only crossed the 5%-line at $1/Gz \approx 0.11$.

Because the experimental data of Meyer and Everts [31] were also for simultaneously hydrodynamically and thermally developing flow, the trend of the local Nusselt numbers correlated better with the correlation of Shah and London [60]. It was found that at $1/Gz = 0.05$ (indicated by the black dotted line), only 10% of the experimental data points were within 5% (thus fully developed). It therefore means that $C = 0.05$ (Eq. (13)), as used in most literature, is inaccurate when the flow is simultaneously hydrodynamically and thermally developing. At $1/Gz = 0.12$ (indicated by the orange dotted line), 80% of the experimental data points were within 5% and all the experimental data points within 10%. This corresponded well to the value of $1/Gz \approx 0.11$ where the correlation of Shah and London [60] crossed the 5%-line. At $1/Gz = 0.14$ (indicated by the purple dotted line), all the experimental data points were within 5%.

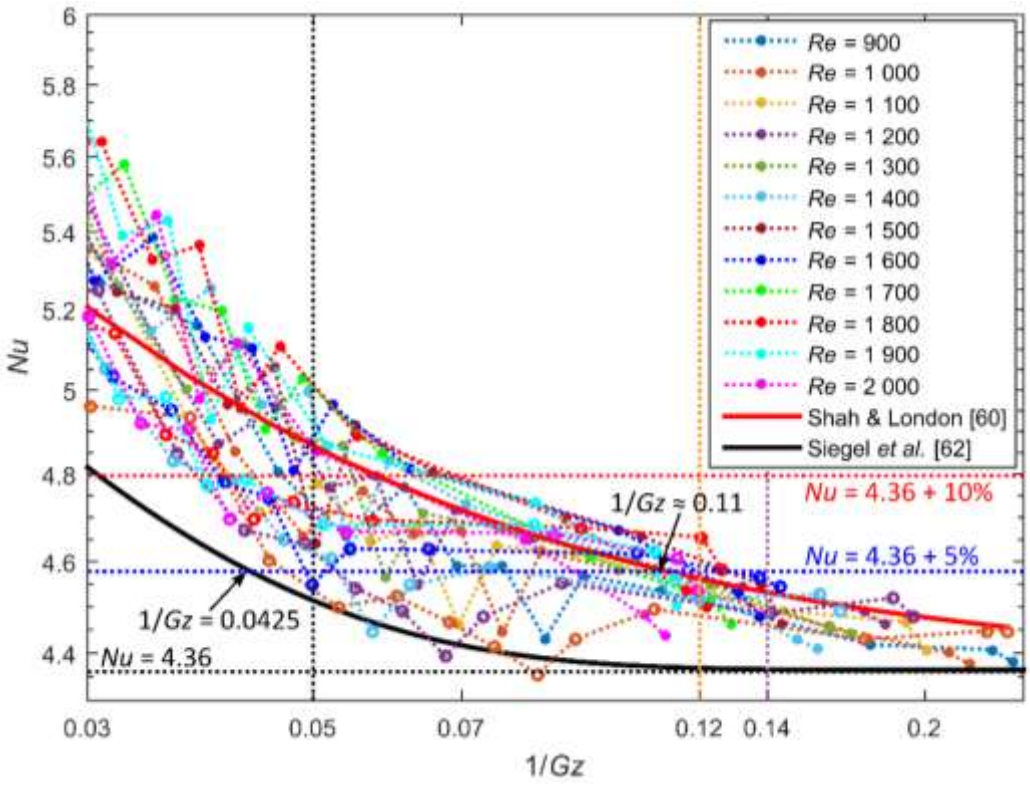

Fig. 2: Local Nusselt numbers as a function of the inverse of the Graetz number for bulk Reynolds numbers between 900 and 2 000 in the 4 mm test section. The filled and empty markers represent the results at heat fluxes of 0.5 kW/m² and 1 kW/m², respectively [31].

Acknowledging the uncertainty of the forced convection experimental data (average uncertainty of 18% and 10% for heat fluxes of 0.5 kW/m^2 and 1 kW/m^2, respectively), Meyer and Everts [31] concluded that $1/Gz \geq 0.12$ is a more accurate/conservative criterion for fully developed flow when

the flow is simultaneously hydrodynamically and thermally developing. A coefficient of 0.05 is therefore better suited for hydrodynamically fully developed flow, while a coefficient of 0.12 was recommended for simultaneously hydrodynamically and thermally developing flow.

The two basic boundary conditions of constant heat flux and constant surface temperature have a significant influence on the magnitude of the fully developed Nusselt numbers in the laminar flow regime, however, the difference decrease with increasing Reynolds numbers and becomes negligible in the turbulent flow regime [47]. Furthermore, the influence of free convection effects is stronger with a constant heat flux boundary condition than with a constant surface temperature boundary condition [5]. It can be postulated that the coefficient of 0.12 may also be suitable to calculate the forced convection thermal entrance length for tubes with a constant surface temperature boundary conditions, because free convection effects are negligible and the boundary condition is not expected to affect the development of the thermal boundary layers along the tube length.

4. Local Heat Transfer in the Laminar and Transitional Flow Regimes

Meyer and Everts [31] concluded that all mixed convection data in the laminar and transitional flow regimes can be represented as shown schematically in Fig. 3. It shows the effect of Grashof number (free convection effects) on the local Nusselt numbers, as a function of axial position, in the laminar flow regime (Fig. 3(a)), on the critical Reynolds number (Fig. 3(b)), and on the laminar-turbulent transition for mixed convection conditions in the transitional flow regime (Fig. 3(d)). The effect of Reynolds number on the laminar-turbulent transition for forced convection conditions in the transitional flow regime is schematically illustrated in Fig. 3(c).

In Figs. 3(a), (b) and (d), the red line 1 represents forced convection conditions, while lines 2 to 4 represent increasing values of Grashof number (thus increased free convection effects). However, in Fig. 3(c), the red dashed line, 1, represents the critical Reynolds number, while lines 2 to 4 represent increasing values of Reynolds number. The reasons why only the trends are shown schematically and not according to scale are [31]: (1) the laminar results of the different Grashof numbers in the FCD region were very close to each other and (2) the FCD region formed only a small part of the tube length, which made it difficult to identify the trends. This was also true for (3) the Nusselt numbers near the inlet of the test section in the transitional flow regime. It was also found that in the transitional flow regime, (4) the laminar-turbulent transition was very dependent on Reynolds number and Grashof number, which made it challenging to obtain and compare results for different Grashof numbers at a fixed Reynolds number, and vice versa. Furthermore, (5) some scatter existed in the experimental data, which made it challenging to illustrate clear trends.

4.1. Laminar flow regime (Fig. 3(a))

If the Grashof number is so low that the flow can be considered as forced convection, the results will follow the red forced convection line. As the flow developes axially from the tube inlet, the thermal boundary layer thickness is a minimum at the inlet of the test section, therefore the Nusselt numbers are highest there. They then decrease along the red forced convection line as the thermal boundary layer thickness increases and the flow approaches fully developed conditions. As the Grashof number increases and free convection effects become significant, the results deviate from the red line. Points D, G and J indicate that the axial position at which the results deviate from the red line (FCD/MCD) decrease with increasing Grashof number.

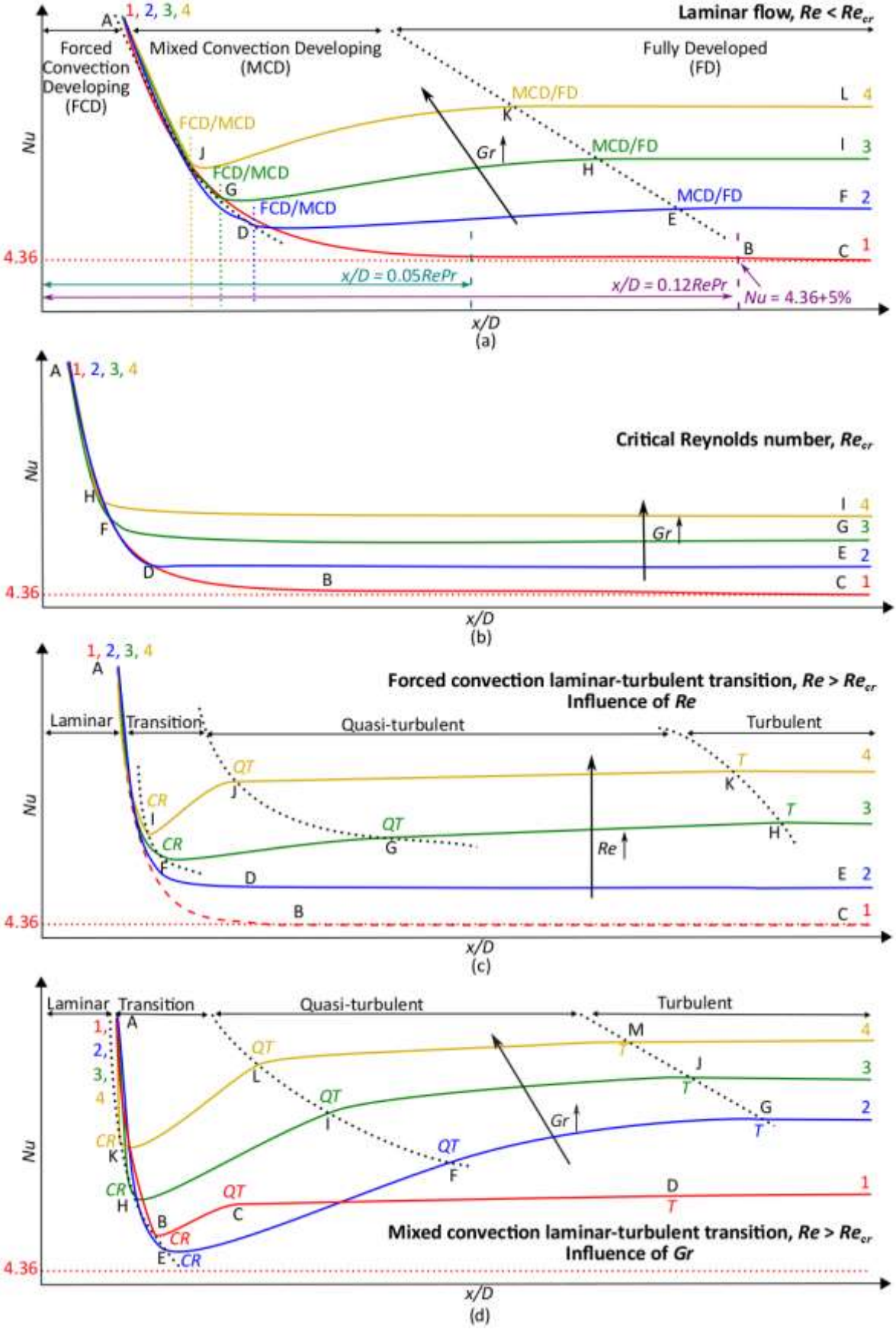

Fig. 3: Schematic representation of the developing Nusselt numbers showing the effects of (a) Grashof number in the laminar flow regime, (b) Grashof number at the critical Reynolds number, (c) Reynolds number on the forced convection laminar-turbulent transition and (d) Grashof number on the mixed convection laminar-turbulent transition [31].

In the forced convection developing (FCD) region, the gradient of the Nusselt numbers decrease slightly with increasing Grashof number, because the thermal entrance length decreases. However, this difference was very small because free convection effects were negligible in this region. In the mixed convection developing (MCD) region, the Nusselt numbers increase along the tube length because the thermal boundary layer and free convection effects increase. As indicated by lines D-E, G-H, and J-K, the gradient of the Nusselt number lines increase with increasing Grashof number due to the increased free convection effects that enhance heat transfer.

Therefore, unlike the forced convection results, the local Nusselt numbers do not decrease and became constant, *but decrease to a minimum and then increase before they become constant and the flow fully developed*. This is due to the combined effects of free convection and flow development. A similar trend was observed by Cheng and Ou [1], who explained that the local Nusselt numbers decrease near the inlet due to the entrance effects and negligible free convection effects. At the minimum Nusselt number (for example, points D, G and J), the entrance and free convection effects are equal, but then the Nusselt numbers begin to increase once the free convection effects begin to dominate the entrance effects. As the flow is not yet fully developed when it begins to deviate from the forced convection line, free convection effects increase along the tube length [24], which causes the Nusselt numbers to increase along the tube length.

As noted earlier, for forced convection conditions, the flow is considered to be fully developed when the Nusselt numbers are within 5% of the theoretical Nusselt number of 4.36. For simultaneously hydrodynamically and thermally developing flow, this corresponds to $x/D = 0.12RePr$ (indicated by the purple dotted line) and not $x/D = 0.05RePr$ (indicated by the teal dotted line). As indicated by points E, H and K, the axial position at which the flow becomes fully developed decreases with increasing Grashof number. In the fully developed (FD) region, the Nusselt numbers and free convection effects are constant along the tube length, because the flow is fully developed. However, the magnitude of the Nusselt numbers increase with increasing Grashof number (points C, F, I and L) due to the increased free convection effects.

4.2. Critical Reynolds number (Fig. 3(b))

The critical Reynolds number corresponds to the Reynolds number before fluctuations in mass flow rate and temperature occur and was obtained using Eq. (1). At the critical Reynolds number, the local Nusselt numbers decrease along the tube length near the inlet of the test section, and then become constant. No MCD regions (Fig. 3(a)) are observed. As the Grashof number increases, the Nusselt number gradients near the inlet of the test section (A-D, A-F and A-H) decrease and the Nusselt numbers become constant at earlier locations along the tube length (points B, D, F and H), because the thermal entrance length decreases. Although the Nusselt numbers remain constant further along the tube length, the magnitude of the Nusselt numbers increase with increasing Grashof number (points C, E, G and I).

4.3. Forced convection laminar-turbulent transition (Fig. 3(c))

The transitional flow regime in terms of fluid velocity (Reynolds number) between the laminar and turbulent flow regimes is caused by the local transition region as a function of axial position. This transition region occurs when the inlet velocity is high enough for mass flow rate and temperature fluctuations to occur, which causes the velocity profile of the fluid to change from laminar to turbulent along the tube length.

When forced convection conditions exist and the Reynolds number exceeds the critical Reynolds number (red and blue lines), the trend is similar to that of the critical Reynolds number. However, the axial position at which the Nusselt numbers becomes constant decreases (points B and D). Furthermore, the magnitude of the Nusselt numbers increases (points C and E) due to the fluctuations inside the test section and the increased fluid velocity that enhances mixing inside the test section.

As the Reynolds number increases further (green and yellow lines), four regions (laminar, transition, quasi-turbulent and turbulent) can be identified. The local Nusselt numbers decrease (laminar) near the inlet of the test section, then increase significantly (transition) with axial position, forming a 'dip'. The heat transfer characteristics in the laminar region are similar to those of the laminar FCD region (Fig. 3(a)). Therefore, the increasing thermal entrance length with increasing Reynolds number causes the gradient of the Nusselt number lines in the laminar region (lines A-F and A-I) to decrease.

The axial position at which the Nusselt numbers start to increase (points F and I), decreases with increasing Reynolds number. In the transitional flow regime, fluctuations occurs inside the test section because the flow alternates between laminar and turbulent flow [63]. Everts and Meyer [24] found that these fluctuations increase along the tube length, leading to increased mixing. Therefore, leading to enhanced heat transfer and increased Nusselt numbers. The gradient of the Nusselt numbers (lines F-G and I-J) increases with increasing Reynolds number, which implies that the transition from the laminar to the quasi-turbulent regions occurs faster (points G and J) and the transition region decreases. Therefore, as the Reynolds number increases in the transitional flow regime, the depth of the dip increases, the width decreases, and the trough (points F and I) occurs earlier.

In the quasi-turbulent region, the flow characteristics are similar to turbulent flow; however, the flow is not yet turbulent and the local Nusselt numbers increase along the tube length. The gradient of the Nusselt number lines in the quasi-turbulent region (lines G-H and J-K) decreases with increasing Reynolds number and approaches zero as the flow approaches the turbulent region. The axial position at which the Nusselt numbers become constant (points H and K) also decreases with increasing Reynolds number, confirming that the transition from laminar to turbulent occurs earlier with increasing Reynolds number. However, as this decrease is less than for points G and J, the width of the quasi-turbulent region increases slightly with increasing Reynolds number. The magnitude of the Nusselt numbers in the quasi-turbulent and turbulent regions increases with increasing Reynolds number due to the enhanced mixing inside the tube.

4.4. Mixed convection laminar-turbulent transition (Fig. 3(d))

When mixed convection conditions exist, the Nusselt numbers decrease along the tube length near the inlet of the test section. As the Grashof number increases, the axial position at which the Nusselt numbers start to increase (points E, H and K) decreases and the gradient of the Nusselt number lines in the transition region (lines E-F, H-I and K-L) increases. Therefore, the width of the transition region decreases with increasing Grashof number.

Although free convection effects cause the flow to transition faster from the laminar to the quasi-turbulent regions (points F, I and L), a significant tube length is still required for the flow to transition to fully turbulent flow. In the quasi-turbulent region, the gradient of the Nusselt number lines (lines F-G, I-J and L-M) decreases with increasing Grashof number and the magnitude of the Nusselt numbers increases. The axial position at which the Nusselt numbers become constant (points G, J and M) decreases with increasing Grashof number. The Nusselt numbers in the turbulent region remain

constant along the tube length because free convection effects remain constant. However, it increases with increasing Grashof number.

Although the laminar-turbulent transition occurs faster with increasing Grashof number when the flow is dominated by mixed convection (blue, green and yellow lines), the trend is different when free convection effects first become significant at very low Grashof numbers (red and blue lines). As free convection effects become significant, the effect is to first disturb the fluctuations inside the test section and cause transition to occur slower. However, at higher Grashof numbers, the fluctuations inside the test section increase significantly with increasing free convection effects [24], which causes the flow to transition faster from laminar to turbulent.

4.5. Boundaries between the FCD, MCD and FD laminar regions

For laminar flow, three different regions (FCD, MCD and FD in Fig. 3(a)) can be defined and correlations were developed to quantify the FCD/MCD and MCD/FD boundaries. The ranges of the correlations are summarised in Table 1.

Table 1: Ranges of correlations to predict the FCD/MCD boundary (Eqs. (14) and (15)) and the MCD/FD boundary (Eqs. (16) and (17)) [31].

	Re	*Pr*	*Gr*	*Gr**	*Gz*	*D* [mm]
FCD/MCD (14), (15)	48 - 3 217	2.9 - 282	2.48 - 4.51×10^5	541 - 4.01×10^6	2.6 - 1.14×10^5	3 - 19
MCD/FD (16), (17)	467 - 3 217	2.9 - 53	30.6 - 4.51×10^5	2.48 – 6.02×10^5	2.6 - 3.49×10^4	4 - 19

4.5.1. FCD/MCD boundary

The FCD/MCD boundary is influenced by mixed convection conditions (*Gr*) and different test fluids (*Pr*). Correlations were developed to calculate the FCD/MCD boundary in terms of the Grashof number and modified Grashof number:

$$Lt_{MCD} = \frac{2.4RePr^{0.6}D}{Gr^{0.57}} \quad (14)$$

$$Lt_{MCD} = \frac{2.1RePr^{0.6}D}{Gr^{*0.45}} \quad (15)$$

Similar to Eq. (13), the FCD/MCD boundary increases with increasing Reynolds number, Prandtl number, and tube diameter, but is inversely proportional to the Grashof number and decreases as free convection effects increase. Furthermore, it is a weaker function of Prandtl number (compared with forced convection) once free convection effects become significant, because the fluid properties (density and viscosity) are accounted for in the Reynolds number and Grashof number.

4.5.2. MCD/FD boundary

It should be noted that the MCD/FD boundary is also the thermal entrance length for mixed convection conditions. Meyer and Everts [31] found that the mixed convection thermal entrance length decreases with increasing free convection effects, therefore both forced convection thermal entrance length conditions ($1/Gz = 0.05$ and $1/Gz = 0.12$) became increasingly inaccurate at higher Grashof numbers. As expected, it was found that the location ($1/Gz$) at which the flow became fully developed decreased significantly with increasing tube diameter (thus increasing Grashof number).

However, for a fixed tube diameter, the value of $1/Gz$ increases with increasing heat flux, because $1/Gz$ is inversely proportional to the Prandtl number, which decreases with increasing temperature.

Correlations were developed to calculate the mixed convection thermal entrance length (MCD/FD boundary) and the correlations were also written as a function of the forced convection thermal entrance length, Lt_{FC}, (using C = 0.12). Those expressions are

$$Lt_{FD} = D\left(\frac{130Re}{Gr^{0.4}Pr^{0.65}}\right)^{10/13} = \frac{Lt_{FC}}{0.12}\left(\frac{130}{Re^{0.3}Pr^{1.95}Gr^{0.4}}\right)^{10/13} \quad (16)$$

$$Lt_{FD} = D\left(\frac{110Re}{Gr^{*\,0.3}Pr^{0.65}}\right)^{10/13} = \frac{Lt_{FC}}{0.12}\left(\frac{110}{Gr^{*\,0.3}Re^{0.3}Pr^{1.95}}\right)^{10/13} \quad (17)$$

4.5.3. Conditions for no MCD region

When higher Prandtl number fluids, such as glycols and nanofluids, are used, the local Nusselt numbers decrease along the tube length and become constant [1, 36, 64-67]. However, the fully developed Nusselt numbers are significantly higher than 4.36, confirming that mixed convection conditions increase the convective heat transfer. In general, the Nusselt numbers also increase with increasing Prandtl number. Because the Nusselt numbers do not increase with axial position before they become constant, the MCD region became negligible and the local Nusselt numbers changed from the FCD region directly to the FD region. This is schematically illustrated by the purple line in Fig. 4. A possible reason for this is that the significantly higher viscosity in the centre of the tube (when high Prandtl number fluids are used), restricts free convection effects to the thermal boundary layer and prevents it from leading to secondary flow, which assists in the diffusion of the heat from the surface to the centre of the tube.

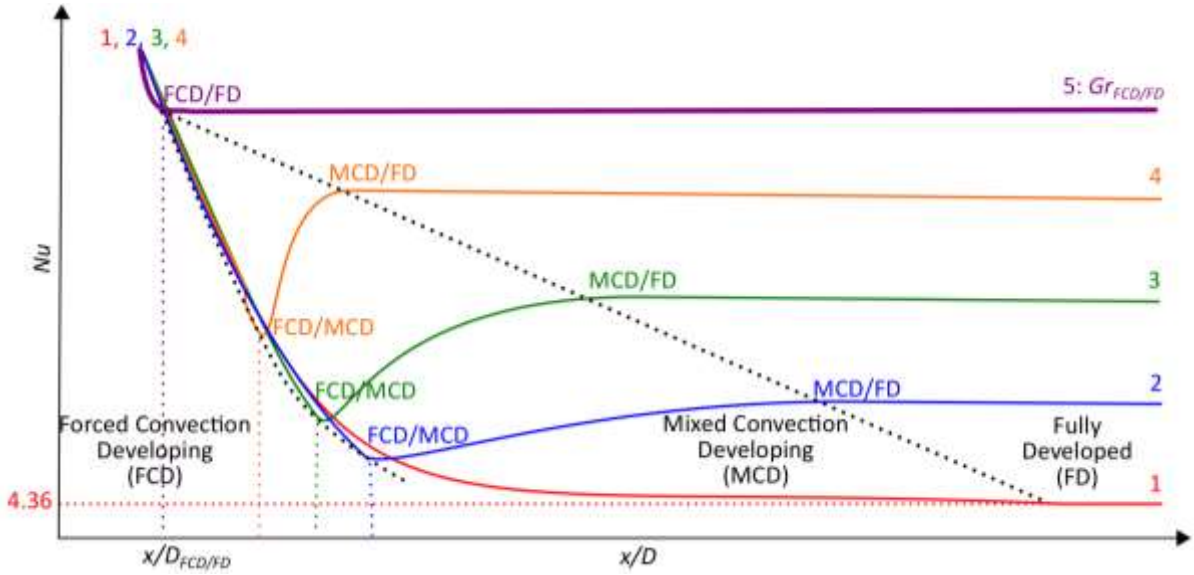

Fig. 4: Schematic representation of the effect of Grashof number on the local Nusselt numbers as a function of axial position, indicating the conditions of no MCD region [31].

The following correlations were developed to determine the Grashof number, $Gr_{FCD/FD}$, (and modified Grashof number, $Gr^*_{FCD/FD}$) for situations where the MCD region is negligible.

$$Gr_{FCD/FD} \geq 1.78 \times 10^{-5} Re^{0.88} Pr^{4.19} \quad (18)$$

$$Gr^{*}_{FCD/FD} \geq 2.03 \times 10^{-6} Re^{1.05} Pr^{5.02} \quad (19)$$

More information on the FCD/FD boundary is available in Meyer and Everts [31].

5. Heat Transfer in the Transitional Flow Regime

Everts and Meyer [24] found that the heat transfer characteristics and boundaries of the transitional flow regime are significantly affected by the axial position along the tube length, free convection effects, and Prandtl number. Based on these influencing parameters, correlations to determine the start and end of the transitional flow regime were developed. For continuity from laminar to turbulent flow, as well as to understand and explain the heat transfer characteristics in the transitional flow regime, the heat transfer characteristics in the laminar, quasi-turbulent and turbulent flow regimes were also briefly investigated.

5.1. Influence of axial position

The influence of axial position was investigated for forced convection conditions to avoid any influences by free convection effects. Due to the very small temperature differences associated with forced convection conditions, the uncertainty of the heat transfer coefficients becomes large at very high Reynolds numbers. Although the Reynolds number was not increased above 6 000, the transitional flow regime, as well as sufficient parts of the laminar and quasi-turbulent flow regimes, was covered. Figure 5 compares the Nusselt numbers and Colburn *j*-factors at a constant heat flux of 1 kW/m^2 in a 4 mm test section as a function of Reynolds number for different axial positions.

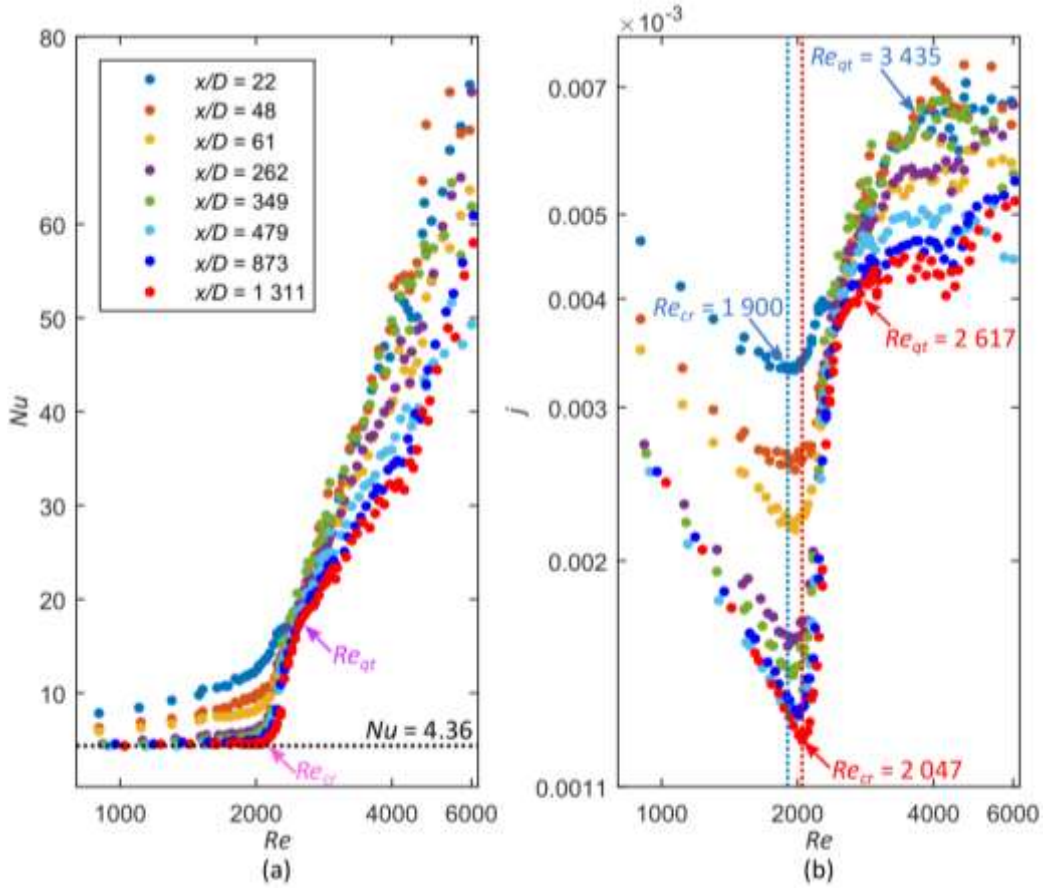

Fig. 5: Comparison of (a) Nusselt numbers and (b) Colburn *j*-factors as a function of Reynolds number at a heat flux of 1 kW/m^2 in a 4 mm test section. The start of the transitional flow regime at *x/D* = 22 and *x/D* = 1 311 is indicated by the vertical dotted lines [24].

The flow was laminar ($(dj/dRe)_L < 0$) between Reynolds numbers of 900 and approximately 2 000 (depending on the tube location). At a fixed Reynolds number, the laminar Nusselt numbers are a maximum near the inlet of the test section (x/D = 22) and then decrease to approximately 4.36 (indicated by the black dotted line) as the flow develops along the tube length. The flow develops for x/D < 479 and free convection effects are negligible [31], thus entrance effects dominate and $(dNu/dRe)_L > 0$ (Eq. (6)). However, the gradient of the laminar Nusselt numbers, $(dNu/dRe)_L$, decreases and approaches zero as x/D increases and the flow approaches fully developed conditions (Eq. (8)). The fully developed ($x/D \geq 479$) laminar Nusselt numbers are in very good agreement (average deviation of 6.4%) with the theoretical fully developed Nusselt number of 4.36.

The vertical dotted lines in Fig. 5(b) indicate that the transitional flow regime starts (Re_{cr}) at a Reynolds number of 1 900 at x/D = 22, and at a Reynolds number of 2 047 at x/D = 1 311. Although it might appear that the start of transition was delayed along the tube length, this was not the case. By investigating the standard deviation of the surface temperatures along the tube length, Everts and Meyer [24] found that transition occurred at the same moment in time along the entire tube length. The increasing critical Reynolds numbers were only due to the temperature gradient along the tube length, and the decreasing viscosity with increasing temperature (this is discussed in more detail Fig. 7). This was confirmed by the isothermal pressure drop results of Everts and Meyer [25] in Fig. 10. When isothermal conditions were investigated, no heat was applied to the test section, therefore no temperature gradient existed and the critical Reynolds numbers along the tube length remained constant.

Although the start of transition is independent of axial position, the end of transition (Re_{qt}) occurs earlier as the flow approaches fully developed conditions. The Colburn j-factors in Fig. 5(b) indicate that the Reynolds number at which transition ended decreases from 3 435 at x/D = 22, to 2 617 at x/D = 1 311. This causes the width of the transitional flow regime (ΔRe) to decrease from a Reynolds number range of 1 535 to 570 and the transition gradient (TG_j in Fig. 1) to increase along the tube length. As indicated in Fig. 3(c), the transition region inside the test section decreases with increasing Reynolds number and a larger portion of the test section contains flow in the quasi-turbulent and turbulent regions. The result is that two fixed axial positions, for example, x/D = 48 and x/D = 1 311, x/D = 48 experiences transition for a wider range of Reynolds numbers, which explains why ΔRe decreases along the tube length. Once the flow is fully developed, ΔRe becomes constant, which explains why there is no significant difference in the transition gradient for x/D > 479 in Fig. 5(b).

The heat transfer coefficients in the quasi-turbulent flow regime are not significantly affected by axial position because the flow is almost turbulent (and thus fully developed). The scatter in the Nusselt numbers and Colburn j-factors in this flow regime is due to the small temperature differences, and thus increased uncertainties. If one thermocouple station measured a slightly higher (or lower) temperature (although it was within the uncertainty of the thermocouple), the Nusselt numbers and Colburn j-factors were also higher (or lower) compared with the rest.

5.2. Influence of free convection

Everts and Meyer [24] thoroughly investigated the influence of free convection on transitional flow by considering not only different heat fluxes, but also different tube diameters and axial positions. To illustrate the effect of free convection on the heat transfer coefficients in the different flow regimes, the Colburn j-factors as a function of Reynolds number are compared in Fig. 6(a) for different heat

fluxes at x/D = 873 in a 4 mm test section and at x/D = 802 in a 11.5 mm test section. Furthermore, the effect of free convection on the heat transfer coefficients in the different flow regimes is schematically illustrated in Fig. 6(b). Points A to N in Fig. 6(a) correspond to the labels used in Fig. 6(b). The results at a constant heat flux of 1 kW/m^2 in the 4 mm test section (line A-B-C in Fig. 6(a)) and the solid black line A-B-C-D-E in Fig. 6(b) represent forced convection conditions, therefore the Grashof numbers were the lowest. The Grashof numbers increased as the heat flux was increased to 3 kW/m^2 in the 4 mm test section (line F-G-H-D) and increased further when the tube diameter was increased to 11.5 mm. Therefore, the maximum Grashof numbers were obtained at a constant heat flux of 3 kW/m^2 in the 11.5 mm test section (line L-M-N-D-E).

It was found that as free convection effects (and thus Grashof number) are increased, due to increasing heat flux (lines A-B and F-G) and tube diameter (lines I-J and L-M), the magnitude of the laminar Colburn j-factors increases and $(dj/dRe)_L$ decreases. It should however be noted that this is only true for the MCD and FD regions. When the heat transfer coefficients fall into the FCD region, entrance effects dominate and free convection effects have a negligible effect (more details available in Everts and Meyer [24]). Because the thermal boundary layer thickness decreases with increasing Reynolds number, the influence of free convection effects decreases with increasing Reynolds number in the laminar flow regime.

Points B and G indicate that the start of transition, Re_{cr}, is delayed from a Reynolds number of 2 005 to 2 163 when the heat flux is increased from 1 kW/m^2 to 3 kW/m^2 in the 4 mm test section. Furthermore, points G and M indicate that, at a fixed heat flux of 3 kW/m^2, transition is significantly delayed from a Reynolds number of 2 163 to 3 176, as the tube diameter is increased from 4 mm to 11.5 mm. The critical Reynolds number therefore increases with increasing Grashof number (free convection effects), as indicated by points B, G, J, M and P in Fig. 6(b). However, it should be noted that free convection effects do not stabilise the flow and delay transition. To clarify this, Fig. 7 compares the surface temperatures and local Reynolds numbers as a function of axial position at the bulk critical Reynolds number at constant heat fluxes of 1 kW/m^2 (forced convection), 3 kW/m^2 and 8 kW/m^2 in a 4 mm test section. As expected, the temperature gradient along the tube length in Fig. 7(a) increases significantly with increasing heat flux. The Reynolds number is inversely proportional to viscosity (which decreases with increasing temperature), therefore the critical Reynolds numbers in Fig. 7(b) increase along the tube length, although transition starts at the same moment in time (same bulk critical Reynolds number) along the entire test section. The critical Reynolds numbers decrease with increasing heat flux for x/D < 95.7 in Fig. 7(b), because free convection effects cause transition to occur earlier (at lower mass flow rates). This was also confirmed by the mass flow rate, temperature and pressure drop fluctuations [24]. However, as x/D is increased further, the increase in critical Reynolds number due to the increased temperature gradients along the test section is more than the decrease due to increased free convection effects, therefore the critical Reynolds numbers increase along the tube length.

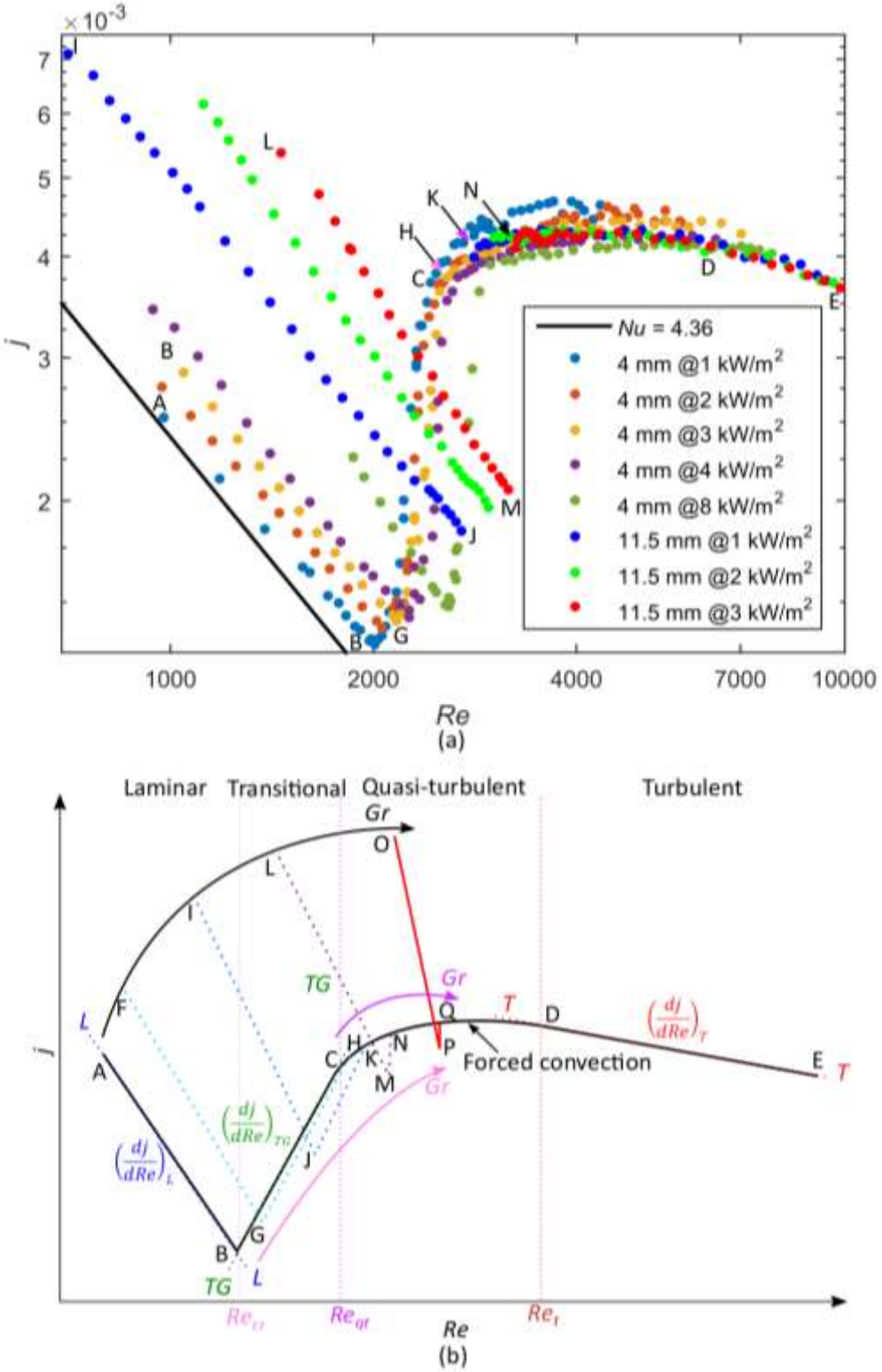

Fig. 6: (a) Comparison of Colburn *j*-factors as a function of Reynolds number for different constant heat fluxes in 4 mm and 11.5 mm test sections and (b) schematic representation of the influence of Grashof number on the different flow regimes when the heat transfer coefficients are investigated in terms of the Colburn *j*-factor as a function of Reynolds number [24].

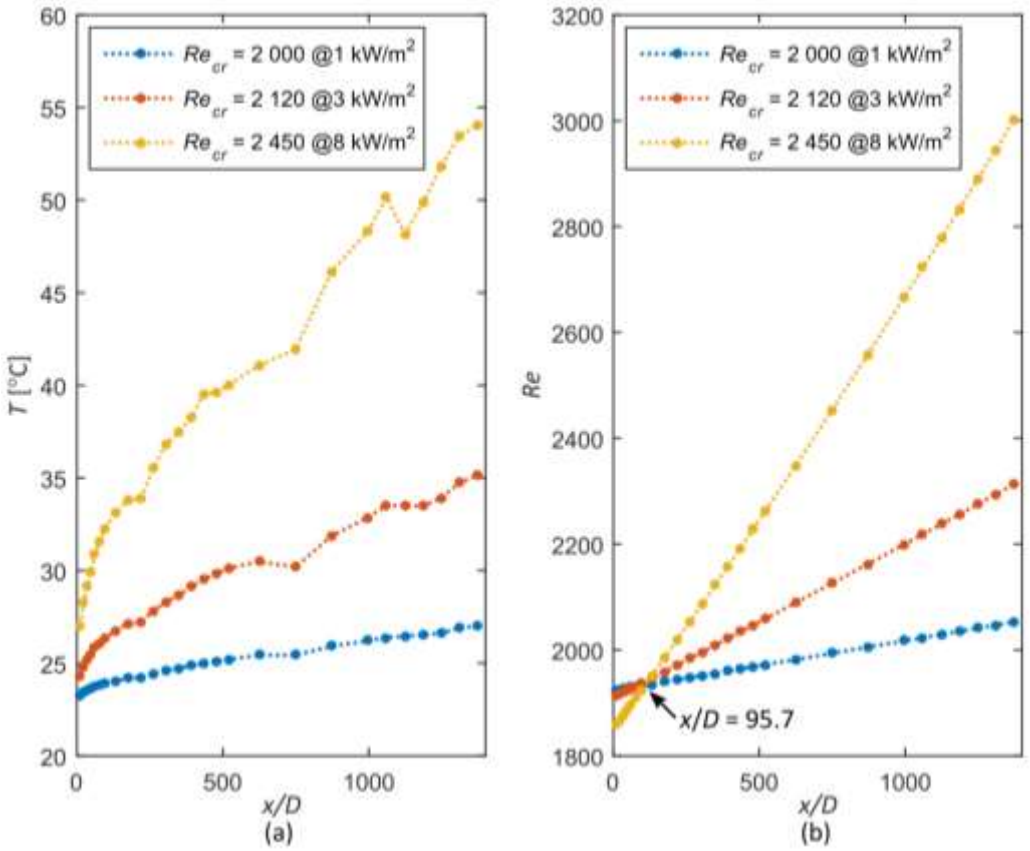

Fig. 7: Comparison of (a) surface temperatures and (b) local Reynolds numbers as a function of axial position at the bulk critical Reynolds number at constant heat fluxes of 1 kW/m² (forced convection), 3 kW/m² and 8 kW/m² in the 4 mm test section [24].

As indicated in Fig. 3(c), free convection effects cause the flow to transition faster from laminar to turbulent along the tube length. Therefore, as the heat flux and tube diameter (Grashof number) are increased, the transition gradient ($(dj/dRe)_{TG}$) in Fig. 6(a) increases from 6.9×10^{-6} at a heat flux of 1 kW/m² in the 4 mm test section (line B-C) to 6.1×10^{-5} at a heat flux of 3 kW/m² in the 11.5 mm test section (line M-N), and the width of the transitional flow regime (ΔRe) decreases from a Reynolds number range of 873 to 35. When the Grashof number is high enough and the flow is fully developed, as in the 11.5 mm test section, the transitional flow regime becomes negligible. The flow alternates between the laminar and quasi-turbulent flow regimes, stabilising as laminar flow at the critical Reynolds number (point M) and in the quasi-turbulent flow regime at the next Reynolds number increment (point N), therefore skipping the entire transitional flow regime.

Although the transitional flow regime becomes negligible, it should be noted that the transition gradient do not tend to infinity ($TG_j \neq \infty$). The reason being that the changes in the *y*-scale (Colburn *j*-factor) are much smaller than the changes in the *x*-scale (Reynolds number). Although the transition gradient remains very small, 7.03×10^{-5}, it is 14.8 times more than the forced convection case in the 4 mm test section. It was not experimentally possible to obtain a Reynolds number increment of less than 35, and the transition gradient will only tend to infinity if the Reynolds number increment tends to zero.

As indicated by points C, H, K and N in Fig. 6(a), an increae in heat flux and tube diameter (thus Grashof number in Fig. 6(b)) delays the end of the transitional flow regime, Re_{qt}. The increased Reynolds numbers are once again due to the decreasing viscosity with increasing temperature. As expected, the

turbulent flow regime is unaffected by heat flux or tube diameter, because the free convection effects are suppressed by the inertia of the fluid. The flow becomes fully turbulent, Re_t, at approximately the same Reynolds number of 6 000 (point D). The the width of the quasi-turbulent flow regime decreases with increasing free convection effects, because the start of the quasi-turbulent flow regime, Re_{qt}, is delayed, while the start of the turbulent flow regime remains unaffected. Everts and Meyer [24] therefore postulated that if the Grashof number is significantly increased and tends to infinity (line O-P-Q-D-E in Fig. 6(b)), the width of both the transitional and quasi-turbulent flow regimes might become negligible for fully developed flow. Therefore, the flow regime might change from laminar to turbulent without any noteworthy transitional and quasi-turbulent flow regimes.

5.3. Influence of Prandtl number

Everts and Meyer [24] investigated the effect of Prandtl number by comparing the results obtained by Strickland [65] at x/D = 192 with the results obtained using water at $x/D \approx 176$ and $x/D \approx 219$ in 4 mm and 11.5 mm test sections in Fig. 8. These thermocouple stations were chosen because they were the closest to x/D = 192, which was used by Strickland [65]. The results of Strickland were obtained using different test fluids and constant heat fluxes (as summarised in Table 2) and are indicated by the square markers, while the results in the 4 mm and 11.5 mm test sections were obtained at a constant heat flux of 3 kW/m^2 and are indicated by the empty and filled circles, respectively.

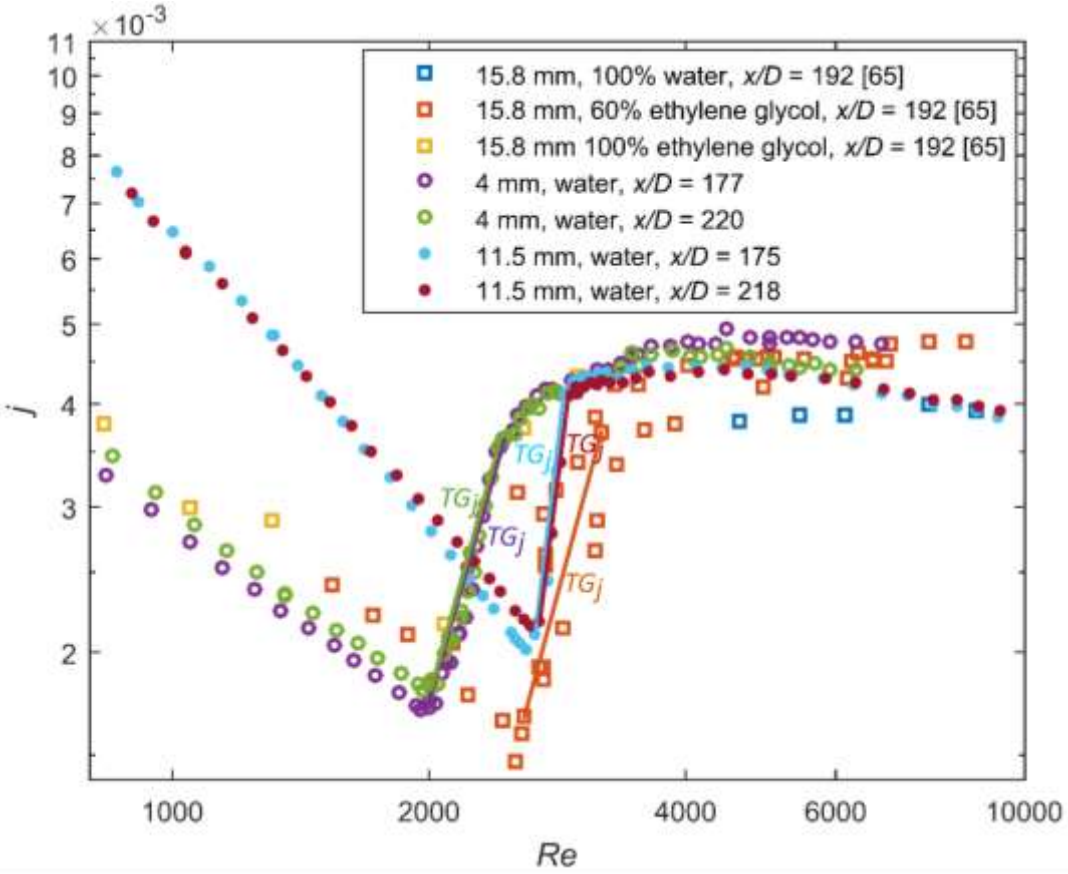

Fig. 8: Comparison of Colburn *j*-factors as a function of Reynolds number of the experimental data of Strickland [65] at x/D = 192 with the experimental data obtained using water at x/D = 177 and x/D = 220 in the 4 mm test section and at x/D = 175 and x/D = 218 in the 11.5 mm test section. The solid lines illustrate the transition gradient of each experimental data set [24].

Table 2: Summary of experimental data of Strickland [65].

	Distilled water	60% ethylene glycol	100% ethylene glycol
Re	3 639 – 50 529	1 180 – 12 456	280 – 3 328
Pr	3.44 – 6.24	16.8 – 55.29	95.89 – 157.8
Nu	31.3 – 232	12.9 – 146.3	15 – 80.2
Gr	$6.3\times10^4 - 2.3\times10^6$	$2.6\times10^3 - 2\times10^5$	$1\times10^3 - 1.6\times10^4$
$\dot{q}$ [kW/m^2]	13.5 – 62.8	4.8 – 57.9	6.1 – 28.8

Although the laminar data of Strickland [65] were obtained at different heat fluxes (4.9 kW/m^2 to 28.8 kW/m^2), Fig. 8 indicates that, unlike the results of Fig. 6(a), the laminar heat transfer coefficients were not affected. This is due to the difference in the fluid properties of water and ethylene glycol. When comparing the fluid properties of water ($Pr \approx 7$) and ethylene glycol ($Pr \approx 100$) between temperatures of 20 °C and 80 °C, it is found that the specific heat and thermal conductivity of ethylene glycol are up to 50% and 60%, respectively, less than water, which lead to greater temperature differences. However, the density is 12% higher and the viscosity an order of magnitude higher than that of water. The viscosity of ethylene glycol is a strong function of temperature, therefore free convection effects are significant, but restricted to the thermal boundary layer (higher temperature and lower viscosity), due to the significantly higher viscosity in the centre of the tube. Free convection effects could therefore not lead to significant secondary flow assists in the diffusion of the heat from the surface to the centre of the tube, and significantly increase the heat transfer coefficients.

For low Prandtl number fluids, such as water, free convection effects lead to a decreased laminar Colburn *j*-factor gradient when the tube diameter is increased from 4 mm to 11.5 mm. Although the tube diameter used by Strickland [65] is 1.37 times and 3.97 times larger than the 11.5 mm and 4 mm test sections, respectively, the Colburn *j*-factor gradient do not decrease significantly because free convection effects are suppressed. The laminar Colburn *j*-factors in the 4 mm test section increase between $x/D = 176$ and $x/D = 219$, because free convection effects increase with increasing thermal boundary layer thickness [31]. However, the difference between the two stations in the 11.5 mm test section is negligible at Reynolds numbers less than 2 000, because the flow is fully developed.

Although the critical Reynolds numbers are expected to increase with increasing heat flux and tube diameter (Fig. 6(a)), transition occurs first in the 4 mm test section ($Re_{cr} = 1\,959$ and $Re_{cr} = 1\,971$), then in Strickland's 15.8 mm test section ($Re_{cr} = 2\,524$), and last in the 11.5 mm test section ($Re_{cr} = 2\,602$ and $Re_{cr} = 2\,637$). Therefore, the increased viscosity of ethylene glycol causes the critical Reynolds number in Strickland's test section to decrease compared with the 11.5 mm test section.

The solid lines in Fig. 8 indicate the transition gradients of each test section. Due to the different heat fluxes and test fluids which were used by Strickland [65], scatter existed in the transitional flow regime; however, the transition gradient was estimated to be 3.38×10^{-6}, while the transition gradients of the 4 mm and 11.5 mm test sections were approximately 4.25×10^{-6} and 9.13×10^{-6}, respectively. Increased free convection effects lead to an increased transition gradient when the tube diameter is increased from 4 mm to 11.5 mm. However, the increased viscosity of 60% ethylene glycol restricts free convection effects to the thermal boundary layer, preventing it from enhancing heat transfer and leading to a faster laminar-turbulent transition along the tube length. Therefore, the transition gradient decreases and the width of the transitional flow regime increases.

The results of the 4 mm and 11.5 mm test sections in the quasi-turbulent and turbulent flow regimes compare fairly well with the results of Strickland [65]. In these flow regimes, free convection effects are suppressed by the inertia of the fluid, therefore the heat transfer coefficients are independent of fluid properties, heat flux and tube diameter. Some scatter and discontinuities are expected in the turbulent flow regime, because the temperature differences decrease, which lead to increased uncertainties.

5.4. Start and end of the transitional flow regime

The Reynolds numbers at which the transitional flow regime started (Re_{cr}) and ended (Re_{qt}) for the results obtained using different tube diameters and heat fluxes, are summarised in Fig. 9(a) to (c), while Fig. 9(d) compares the width of the transition flow regime (ΔRe). In Fig. 9(c), the empty markers represent the start of the transitional flow regime, while the filled markers represent the end of the transitional flow regime.

Although the start of transition is independent of axial position (Section 5.1) and occurs earlier with increasing free convection effects (Section 5.2), the critical Reynolds numbers in Fig. 9(a) increase along the tube length and the gradient increases with increasing heat flux and tube diameter. Furthermore, the start of transition occurs significantly earlier in the 4 mm test section ($Re_{cr} \approx 1\,900$) than in the 11.5 mm test section ($Re_{cr} \approx 2\,500$). There are two possible reasons for this: (1) Reynolds number is proportional to tube diameter and therefore increases with increasing tube diameter. (2) A greater contraction ratio (ratio of the flow-calming section diameter to the test section diameter) to the 4 mm test section causes a different disturbance of the boundary layer at the inlet of the test section, which causes transition to occur earlier. The contraction ratio in the 4 mm test section was 60.5, while it was 14.9 in the 11.5 mm test section, and approximately 10 in the work of Ghajar and co-workers [3, 5-7, 10, 14, 15, 65].

Fig. 9(b) indicates that the Reynolds number at which transition ends decreases significantly with increasing axial position near the inlet of the test section, but then increases further along the tube length. Furthermore, Fig. 9(d) indicates that the width of the transitional flow regime, ΔRe, decreases along the tube length when the flow is developing, and remains approximately constant once the flow is fully developed. Because transition started at the same moment in time along the entire test section and ΔRe decreased along the test section, it was concluded that Re_{qt} occurred earlier as the flow developed along the tube length, but at the same moment in time once the flow was fully developed. This is as expected because Fig. 3(c) and (d) indicate that the transition region inside the test section decreases with increasing Reynolds number (fluid velocity) and/or Grashof number (free convection effects). Therefore, at a fixed Reynolds number, part of the test section could be in the transition region, while the remaining part of the test section could already be in the quasi-turbulent or even turbulent region.

Everts and Meyer [24] divided the transitional flow characteristics along the tube length into three regions. Because these regions are affected by free convection effects, it was only indicated for the forced convection case (1 kW/m^2 in the 4 mm test section) in Fig. 9(d). In Region 1, ΔRe decreases significantly along the tube length due to the increasing thermal boundary layer thickness. Free convection effects have a negligible influence on ΔRe because the thermal boundary layer thickness remains very small. In Region 2, the thermal boundary layer thickness is sufficient for free convection effects to become significant. Therefore, ΔRe decreases with axial position (due to the increasing

thermal boundary layer thickness and increasing mass flow rate and temperature fluctuations). It also decreases with increasing heat flux and tube diameter, because free convection effects cause the flow to transition faster from laminar to turbulent. Δ*Re* becomes independent of axial position when the flow is fully developed (Region 3). However, it decreases significantly with increasing free convection effects (heat flux and tube diameter) and becomes negligible when the Grashof number is very high (3 kW/m^2 in the 11.5 mm test section). The reason being that free convection effects cause the transition region (in terms of axial position) to decrease and become negligible at the end of the test section (where the flow is fully developed). Therefore, the transitional flow regime (in terms of Reynolds number) becomes negligible when the flow is fully developed.

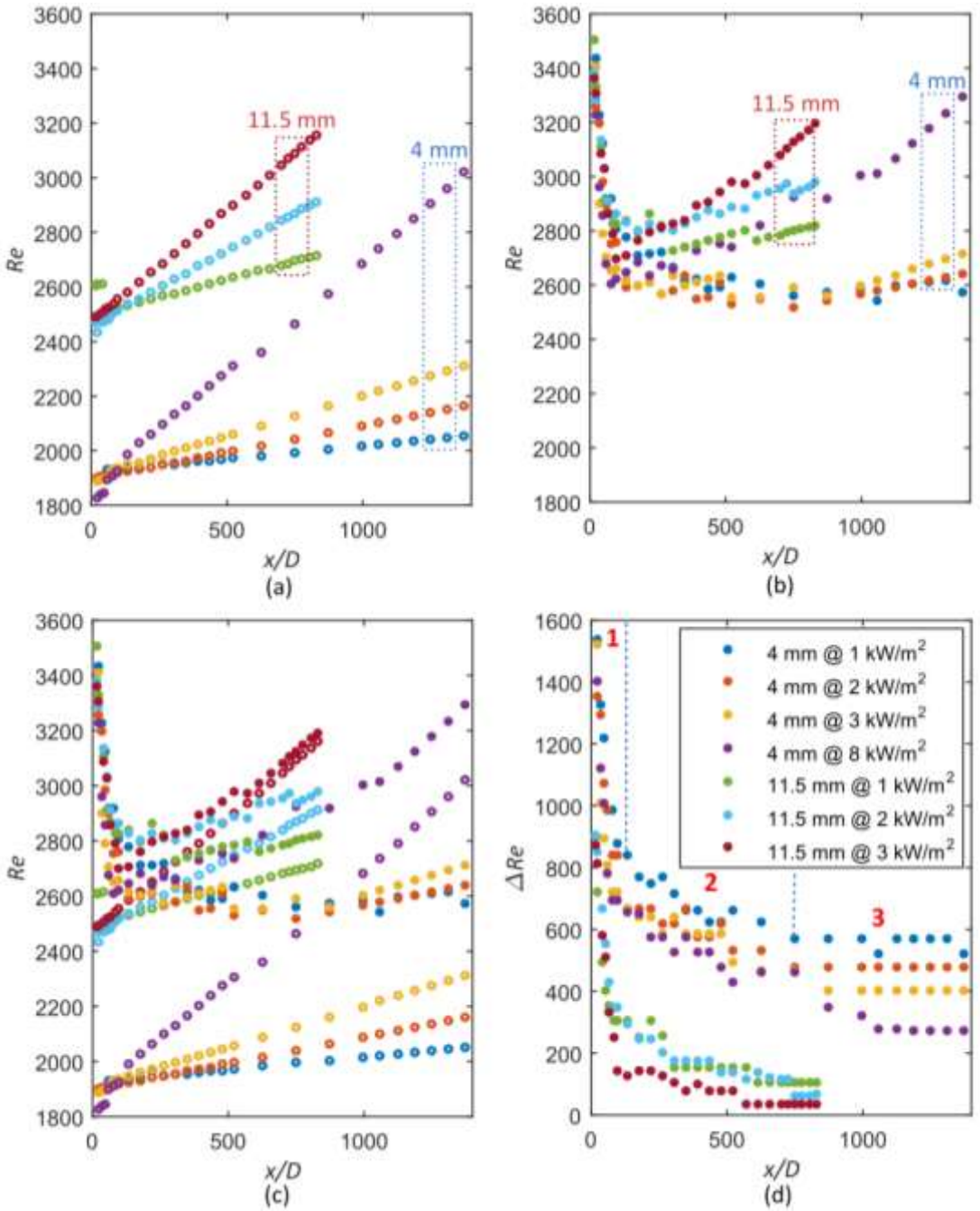

Fig. 9: Comparison of (a) Reynolds numbers at which transition starts, (b) Reynolds numbers at which transition ends, (c) Reynolds numbers at which transition starts and ends and (d) width of the transitional flow regime, as a function of axial position for different constant heat fluxes in the 4 mm and 11.5 mm test sections. In Fig. 9(c), the empty markers represent the start of transition, while the filled markers represent the end of transition [24].

It should be noted that for forced convection conditions (1 kW/m^2 in the 4 mm test section), Δ*Re* gradually decreases and becomes constant at a Reynolds number range of 570 at *x*/*D* = 748. As the heat flux (and thus free convection effects) was increased, the axial position at which Δ*Re* became constant increased, while the opposite trend was observed in the 11.5 mm test section. For the 4 mm test section, the average Grashof number in the transitional flow regime was approximately 100 at a heat flux of 1 kW/m^2, and increased to 500 and 2 000 as the heat flux was increased to 3 kW/m^2 and 8 kW/m^2, respectively. In the 11.5 mm test section, the average transitional Grashof number at heat fluxes of 1 kW/m^2 and 3 kW/m^2 was approximately 7 000 and 15 000, which was an order of magnitude more than in the 4 mm test section. As indicated in Fig. 3(d), free convection effects initially disturb the fluctuations inside the test section and cause transition to occur slower compared with forced convection conditions. However, as the Grashof number is increased further, the fluctuations are enhanced and transition occurs faster.

Everts and Meyer [24] developed the following correlations to predict the start and end of the transitional flow regime for mixed convective developing and fully developed flow with a square-edged inlet:

$$Re_{cr} = \left(0.1972\frac{x}{D} + 1156.7\right) Gr^{0.077} \quad (20)$$

$$Re_{cr} = \left(0.209\frac{x}{D} + 1044.4\right) Gr^{*0.07} \quad (21)$$

The correlations indicate that the critical Reynolds number increases linearly along the test section (due to the decreasing viscosity with temperature) and the gradient of the line is influenced by the Grashof number, thus free convection effects. Furthermore, the following correlations were developed to predict the end of the transitional flow regime for developing and fully developed flow [24]:

$$Re_{qt} = 2504\ Gr^{0.018} \quad (22)$$

$$Re_{qt} = 2313.2\ Gr^{*\,0.02} \quad (23)$$

Although Eqs. (22) and (23) are suitable for developing flow, it was not necessary to include the axial position (*x*/*D*), because the Grashof number is a function of tube location (temperature difference and thermal properties vary along the tube length).

Everts and Meyer [24] compared Eqs. (20)-(23) with their experimental data as well as results in literature, and the performance and ranges of the correlations are summarised in Table 3. The Re_{cr} correlations could predict 80% of the data within 10% and approximately all the data within 20%. The Re_{qt} correlations could predict 85% of the data within 10% and the average deviation was approximately 6%.

Table 3: Overall performance and ranges of the correlations to predict the start and end of the transitional flow regime for a square-edged inlet [24].

	Eq.	Everts and Meyer [24]				Everts and Meyer [24] and literature [28]			
		n	±10% [%]	±20% [%]	Ave %	*n*	±10% [%]	±20% [%]	Ave %
Re_{cr}	*Gr*: (20)	212	83	99.5	6.1	272	81	99.6	6.6
	*Gr**: (21)	212	82	99.5	5.8	272	80	99.6	6.4
		$1\,828 \le Re \le 3\,158$, $3.8 \le Pr \le 6.9$, $923 \le Gr \le 7.62\times10^4$, $1.08\times10^3 \le Gr^* \le 1.11\times10^6$, $13.63 \le x/D \le 1\,373$, $4\text{ mm} \le D \le 11.5\text{ mm}$				$1\,828 \le Re \le 3\,158$, $3.8 \le Pr \le 6.9$, $923 \le Gr \le 2.62\times10^5$, $1.08\times10^3 \le Gr^* \le 4.42\times10^6$, $12.63 \le x/D \le 1\,373$, $4\text{ mm} \le D \le 19\text{ mm}$			
Re_{qt}	*Gr*: (22)	212	89	99.5	5.6	272	85	99	6.1
	*Gr**: (23)	212	89	99.5	5.6	272	85	99	6.1
		$2\,519 \le Re \le 3\,506$, $4 \le Pr \le 7.5$, $28 \le Gr \le 5.76\times10^4$, $1.1\times10^3 \le Gr^* \le 8.36\times10^5$, $13.63 \le x/D \le 1\,373$, $4\text{ mm} \le D \le 11.5\text{ mm}$				$2\,365 \le Re \le 4\,287$, $4 \le Pr \le 7.5$, $28 \le Gr \le 6.14\times10^4$, $1.1\times10^3 \le Gr^* \le 1.46\times10^6$, $13.63 \le x/D \le 1\,373$, $4\text{ mm} \le D \le 19\text{ mm}$			

6. Pressure Drop in the Transitional Flow Regime

To investigate the pressure drop characteristics of developing and fully developed flow, Everts and Meyer [25] measured the pressure drop across eight different tube lengths along a test section. The isothermal friction factors as a function of bulk Reynolds number for different tube lengths are compared in Fig. 10. The pressure drop increases with increasing fluid velocity; however, the friction factors decrease with increasing Reynolds number, because it is inversely proportional to the velocity squared ($f = 2\Delta PD/(L\rho V^2)$). At a fixed Reynolds number of 2 000, the laminar friction factors decrease and approach the solid blue line ($64/Re$) as the tube length increases, because a larger portion of the tube length contains fully developed flow. In general, the friction factors of developing flow are higher than for fully developed flow, because the maximum wall shear stress is found at the inlet of the test section where the hydrodynamic boundary layer is the thinnest. Once the flow is fully developed, for example, over the last part of the test section ($8\text{ m} < L < 9.5\text{ m}$), the friction factors correspond very well to $64/Re$ (average deviation of 2.5%). This trend is clear for Reynolds numbers larger than 2 000, but challenging to identify for Reynolds numbers less than 1 000, due to the uncertainties of the friction factors that increase with decreasing Reynolds numbers.

Transition started at the same Reynolds number of 2 361 for all tube lengths, confirming that the start of transition is independent of tube length (thus developing and fully developed flow). However, the Reynolds number at which transition ended decreased from 2 809 for $0\text{ m} < L < 2\text{ m}$, to 2 622 for $8\text{ m} < L < 9.5\text{ m}$ (fully developed flow). Because transition ends earlier as the flow develops along the tube length, the transition gradient increases and the width of the transitional flow regime decreases. The detailed view in Fig. 10 indicates that the transition gradient, TG_f, near the inlet of the test section ($0\text{ m} < L < 2\text{ m}$) was approximately 1.9×10^{-5} and it increased to approximately 4.6×10^{-5} when the flow was fully developed ($8\text{ m} < L < 9.5\text{ m}$).

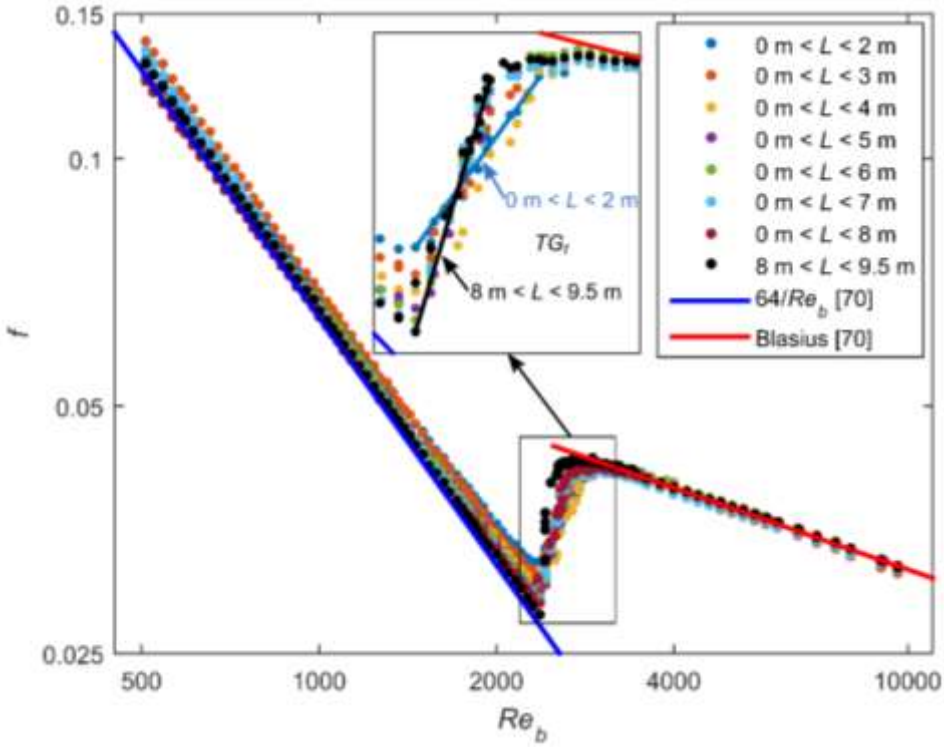

Fig. 10: Comparison of isothermal friction factors as a function of bulk Reynolds number across different tube lengths [25].

Everts and Meyer [25] also investigated the effect of free convection on the friction factors of developing and fully developed flow by comparing different heat fluxes and tube lengths in Fig. 11. Similar to the results obtained by Tam and Ghajar [15], the laminar friction factors increase slightly with increasing heat flux. This trend becomes more prominent as the tube length is increased and the flow approaches fully developed flow (Fig. 11(h)), because free convection effects increase with increasing thermal boundary layer thickness. Tam and Ghajar [15] explained that the velocity profile changes when mixed convection occurs. As the heat flux is increased, the density decreases, and the shear stress due to the change in the velocity profile increases, which leads to increased friction factors. Furthermore, the decreasing viscosity leads to increased Reynolds numbers (Fig. 7). Therefore, when the flow is fully developed (8 m < L < 9.8 m in Fig. 11(h)) at a fixed Reynolds number of approximately 1 650, the viscosity decreased by 32% when the heat flux was increased from 1 kW/m^2 to 3 kW/m^2, while the mass flow rate (thus fluid velocity) decreased by approximately 35%. Although the decreased density and viscosity caused the pressure drop across the tube length to decrease by 50%, the significantly lower fluid velocities caused the friction factors to increase by 13% ($f \propto 1/V^2$). However, when the viscosity decreases significantly with temperature (for example when ethylene glycol is used), the decrease in pressure drop might be more than the increase due to the decreased fluid velocity, which will then lead to decreased friction factors (as was found by Tam *et al*. [10]).

The black rectangle in Fig. 11(h) indicates that a discontinuity existed between Reynolds numbers of 2 700 and 2 900. This was due to the different pressure transducer diaphragms that were used to conduct experiments between Reynolds numbers of 500 and 4 000, and between 2 000 and 10 000. At a Reynolds number of 2 880, friction factors of 0.02596 and 0.02368 were obtained using the two different pressure transducer diaphragms. Because this difference was only 1.6%, which is less than the friction factor uncertainty of approximately 5% at this heat flux and Reynolds number, it was considered to be negligible. Slight discontinuities existed in the friction factors of the other tube lengths as well; however, it was even less due to the longer tube lengths and lower uncertainties.

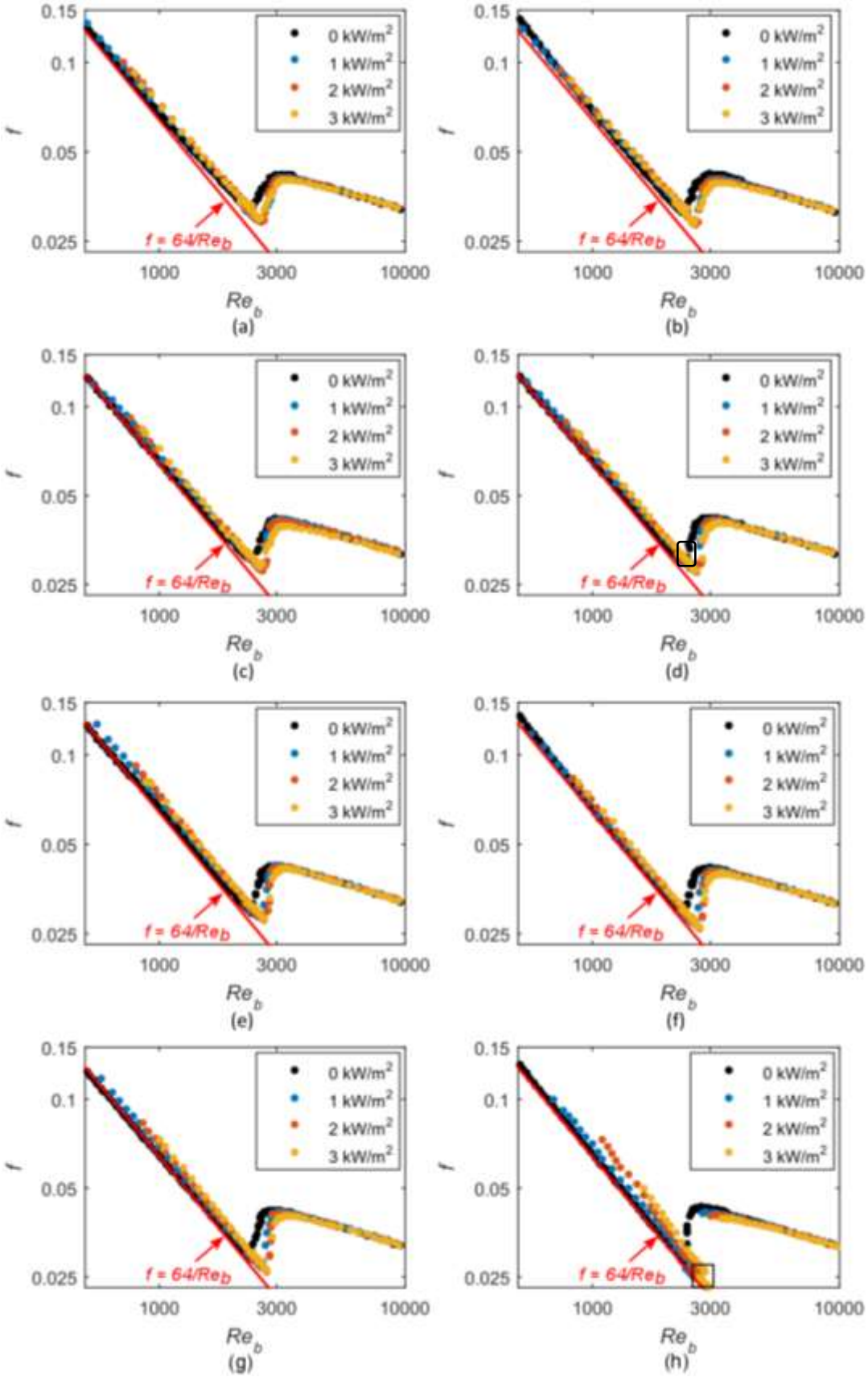

Fig. 11: Comparison of friction factors as a function of bulk Reynolds number at different constant heat fluxes across (a) 0 m ≤ *L* ≤ 2 m, (b) 0 m ≤ *L* ≤ 3 m, (c) 0 m ≤ *L* ≤ 4 m, (d) 0 m ≤ *L* ≤ 5 m, (e) 0 m ≤ *L* ≤ 6 m, (f) 0 m ≤ *L* ≤ 7 m, (g) 0 m ≤ *L* ≤ 8 m and (h) 8 m ≤ *L* ≤ 9.5 m. The heat flux of 0 kW/m² indicates isothermal flow. The black rectangle in Fig. 11(h) indicates the region where different pressure transducers had to be used because of pressure transducer diaphragm range limitations [25].

Although free convection effects cause transition to occur at lower mass flow rates, the decreasing viscosity with increasing temperature causes the critical Reynolds numbers to increase with increasing heat flux (Fig. 7). Near the inlet of the test section (0 m < L < 2 m in Fig. 11(a)), transition started at Reynolds numbers of 2 520 and 2 532 at heat fluxes of 1 kW/m^2 and 3 kW/m^2, respectively. However, when the flow was fully developed (8 m < L < 9.5 m in Fig. 11(h)), transition was delayed to Reynolds numbers of 2 641 and 3 142 for heat fluxes of 1 kW/m^2 and 3 kW/m^2, respectively. The difference between the critical Reynolds numbers of the two heat fluxes increased along the tube length from a Reynolds number range of 12 (Fig. 11(a)) to 541 (Fig. 11(h)), due to the increased temperature gradient along the test section with increasing heat flux (Fig. 7).

Similar to the isothermal results, the transition gradient increases with increasing tube length (flow approaches fully developed flow), which causes the width of the transitional flow regime, ΔRe, to decrease. Furthermore, ΔRe decreases with increasing heat flux, because free convection effects cause the flow to transition faster from laminar to turbulent along the tube length (Fig. 3). This leads to a decreased transition region along the test section, and also a decreased transitional flow regime in terms of Reynolds number (Fig. 6(b)). Once the flow is fully developed and free convection effects are significant, the transitional flow regime becomes negligible and it seems as if $TG_f \rightarrow \infty$ at Re_{cr} in Fig. 11(h). However, this is not the case because the changes in the y-scale (friction factor) are much smaller than the changes in the x-scale (Reynolds number). TG_f remains a small value of 4.2×10^{-5}, but it is 4.6 times greater than for 0 m < L < 2 m (Fig. 11(a)). Similar to the local heat transfer results in Fig. 6(a), severe fluctuations occurs inside the test section and after time (up to one hour), the flow stabilises at the critical Reynolds number and then in the quasi-turbulent flow regime at the next increasing experimental Reynolds number increment.

As expected, there is no significant difference between the results of the different tube lengths and heat fluxes in the quasi-turbulent and turbulent flow regimes, because the flow is fully developed and free convection effect are suppressed by the velocity of the fluid.

7. Relationship between Pressure Drop and Heat Transfer

When surface temperature and pressure drop measurements are taken simultaneously during experiments, the relationship between pressure drop and heat transfer can be investigated. For example, Fig. 12 compares the average friction factors and Colburn j-factors for 0 m < L < 8 m at constant heat fluxes of 1 kW/m^2 and 3 kW/m^2. The boundaries of the different flow regimes (Re_{cr}, Re_{qt} and Re_t) are indicated by the dotted lines (coloured according to the heat flux).

This figure indicates that the trends of the friction factors and Colburn j-factors are very similar. In the laminar flow regime, the friction factors and Colburn j-factors decrease with increasing Reynolds number. At a fixed Reynolds number of 2 370, the increase in friction factors between the two heat fluxes was 4%, while the increase in Colburn j-factors was 29%. Therefore, free convection effects have a greater influence on the heat transfer coefficients than on the friction factors in the laminar flow regime.

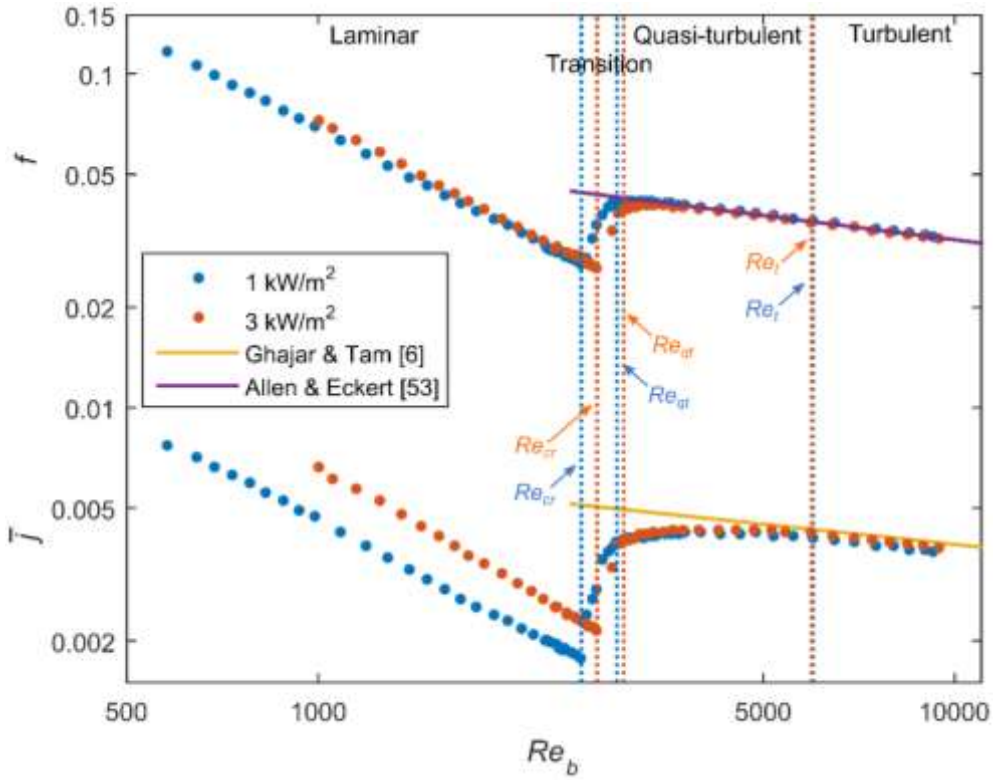

Fig. 12: Comparison of the pressure drop and heat transfer results in terms of the friction factors and average Colburn *j*-factors for 0 m < *L* < 8 m as a function of bulk Reynolds number at constant heat fluxes of 1 kW/m² and 3 kW/m² [25].

At a heat flux of 3 kW/m^2, the gradients of both friction factors (df/dRe) and Colburn *j*-factors (dj/dRe) changed from negative to positive at a Reynolds number of 2 740, which indicates the start of the transitional flow regime (Re_{cr}). Both friction factors and Colburn *j*-factors increase with increasing Reynolds number in the transitional flow regime. Transition ended (Re_{qt}) at a Reynolds number of approximately 3 019, where the gradient of both the friction factor and the Colburn *j*-factor lines decreases compared with the transitional flow regime ($(df/dRe)_{QT} < (df/dRe)_{TG}$ and $(dj/dRe)_{QT} < (dj/dRe)_{TG}$).

In the quasi-turbulent flow regime, both the friction factors and Colburn *j*-factors first increase with increasing Reynolds number (although the gradients are significantly less than in the transitional flow regime), and then decrease as the Reynolds number is increased further, forming a concave curve. The concave curve of the Colburn *j*-factors is flatter than for the friction factors, because the gradient of the Colburn *j*-factors is less than for the friction factors. Near the end of the quasi-turbulent flow regime, the trends of the friction factors and Colburn *j*-factors are similar to the turbulent flow regime (decrease with increasing Reynolds number); however, it is not fully turbulent yet. The Colburn *j*-factors indicate that the flow only became fully turbulent (Re_t) at a Reynolds number of approximately 5 955, where both friction factors and Colburn *j*-factors decrease with increasing Reynolds number and correlate very well with the correlations of Allen and Eckert [53] and Ghajar and Tam [6]. This corresponds well to Re_t = 6 000, which was obtained by Everts and Meyer [24].

Everts and Meyer [25] therefore concluded that the boundaries of the different flow regimes, especially the transitional flow regime, were the same for pressure drop and heat transfer for all the experiments. However, Tam *et al*. [10] found that the transition region, ΔRe, was wider for heat transfer than for pressure drop. A possible explanation is that Tam *et al*. [10] considered the quasi-turbulent flow regime as part of the transitional flow regime when the Colburn *j*-factors were

investigated, while it was considered as part of the turbulent flow regime when the friction factors were investigated.

The relationship between pressure drop and heat transfer can be quantified by dividing the friction factors by the Colburn *j*-factors (*f*/*j*-factors). For example, the *f*/*j*-factors for tube lengths of 0 m < *L* < 2 m (Fig. 11(a)) and 0 m < *L* < 8 m (Fig. 11(g)), at a constant heat flux of 3 kW/m^2 are compared in Fig. 13. The laminar *f*/*j*-factors increase with increasing Reynolds number and are affected by developing flow and free convection effects. In the transitional flow regime, the *f*/*j*-factors decrease significantly with increasing Reynolds number; however, this decrease is slightly less for 0 m < *L* < 2 m than for 0 m < *L* < 8 m. Although the *f*/*j*-factors continue to decrease in the quasi-turbulent flow regime, the gradient increases compared with the transitional flow regime, and approaches zero in the turbulent flow regime. Furthermore, as the Reynolds number is increased, the difference in the *f*/*j*-factors of the two tube lengths decreases, and becomes negligible in the turbulent flow regime, because the flow is fully developed and free convection effects are suppressed. Everts and Meyer [25] therefore concluded that the *f*/*j*-factors in the laminar flow regime are a function of Grashof number (free convection effects), while it is a function of Reynolds number in the other flow regimes.

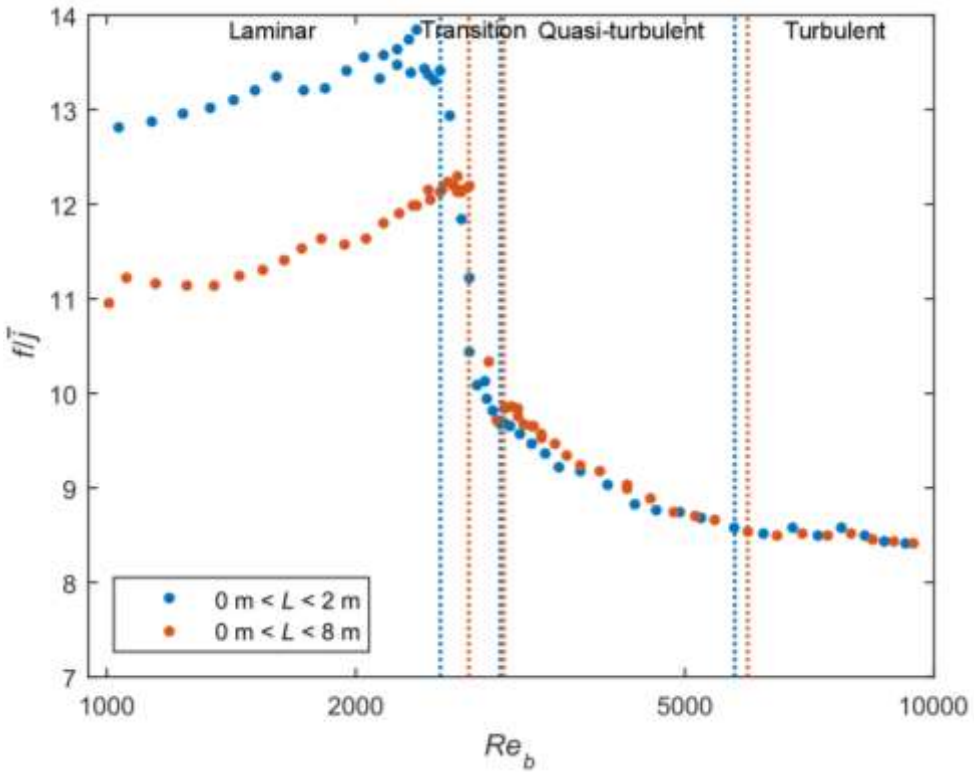

Fig. 13: Comparison of the friction factors divided by the average Colburn *j*-factors as a function of bulk Reynolds number for 0 m < *L* < 2 m and 0 m < *L* < 8 m at a constant heat flux of 3 kW/m^2 [25].

It was also noted that the *f*/*j*-factors can be used to identify the boundaries of the different flow regimes, in addition to the criteria presented in Section 2.1 [25]. Furthermore, it will also ensure a better understanding of the trade-off between pressure drop and heat transfer in the different flow regimes. Everts and Meyer [25] developed correlations that quantify the relationship between pressure drop and heat transfer (*f*/*j*-factors) of developing and fully developed flow in the different flow regimes. The Colburn *j*-factor ($j = Nu/(RePr^{1/3})$) can then be substituted to obtain friction factor correlations as a function of average Nusselt number, or vice versa. It should be noted that although

the correlations are not explicitly a function of tube length, *L*, they are valid for developing and fully developed flow, because the bulk Reynolds number, Grashof number and Prandtl number for tube length *L*(*x*) are used.

The relationship between pressure drop and heat transfer in the laminar flow regime is a function of free convection effects, therefore the following correlations were developed:

$$\frac{f}{\bar{j}} = 109.71 Gr_b^{-0.215} \quad (24)$$

$$\frac{f}{\bar{j}} = 115.01 Gr_b^{*-0.179} \quad (25)$$

By substituting the Colburn *j*-factor, the following correlations are obtained to calculate the friction factor as a function of average Nusselt number and bulk Grashof number (or modified Grashof number):

$$f = \frac{109.71\,\overline{Nu}}{Re_b Pr_b^{1/3} Gr_b^{0.215}} \quad (26)$$

$$f = \frac{115.01\,\overline{Nu}}{Re_b\, Pr_b^{1/3} Gr_b^{*0.179}} \quad (27)$$

Because the *f*/*j*-factors in the transitional, quasi-turbulent and turbulent flow regimes are a stronger function of Reynolds number than Grashof number, a single correlation for these three flow regimes was developed:

$$\frac{f}{\bar{j}} = \left(\frac{3.74\,Re_b - 8066}{Re_b - 2320}\right) Pr_b^{0.42} \quad (28)$$

$$f = \left(\frac{3.74\,Re_b - 8066}{Re_b - 2320}\right) \frac{\overline{Nu}}{Re_b Pr_b^{0.087}} \quad (29)$$

Table 4 indicates that the laminar friction factor correlations could predict approximately all their experimental data within 5%, while a single correlation for the transitional, quasi-turbulent and turbulent flow regimes could predict almost all the data (97%) within 10%.

Table 4: Summary of the ranges and performance of the friction factor correlations [25].

	Eq.	Data points	±5% [%]	±10% [%]	±20% [%]	Ave [%]	Range
Friction factors							
Laminar	(26	495	92	100	100	2.4	467 ≤ *Re* ≤ 3 217, 3 ≤ *Pr* ≤ 7.4, 2.6 ≤ *Gr* ≤ 5 589, 541 ≤ *Gr** ≤ 4.01×10^6
	(27	495	95	100	100	2.2	
Transitional, quasi-turbulent and turbulent	(29	834	85	97	99.9	2.8	2 483 ≤ *Re* ≤ 9 787, 5.4 ≤ *Pr* ≤ 6.9, 8.9×10^2 ≤ *Gr* ≤ 3.2×10^4, 5.9×10^4 ≤ *Gr** ≤ 3.7×10^5

8. Nusselt Number Correlations: Laminar, Transitional, Quasi-turbulent and Turbulent Flow

Meyer and Everts [31] developed the following correlations that accurately predicts the local Nusselt numbers in all three laminar regions (FCD, MCD and FD in Fig. 3(a)):

$$Nu = 4.36 + (Nu_1^6 + Nu_2^6)^{1/6} \quad (30)$$
$$Nu_1 = (0.33Gz^{0.54} - 0.84)Pr^{-0.2}$$
$$Nu_2 = (0.207Gr^{0.305} - 1.19)Pr^{0.5}Gz^{-0.08}$$

$$Nu = 4.36 + (Nu_1^6 + Nu_2^6)^{1/6} \quad (31)$$
$$Nu_1 = (0.33Gz^{0.54} - 0.84)Pr^{-0.2}$$
$$Nu_2 = (0.202Gr^{*\,0.254} - 1.23)Pr^{0.45}Gz^{-0.06}$$

By intergrating these correlations, Meyer and Everts [31] proposed the following correlation to calculate the average laminar Nusselt number over a length, *L*, measured from the tube inlet:

$$\overline{Nu} = 4.36 + \overline{Nu}_1 + \overline{Nu}_2 \quad (32)$$

$$\overline{Nu}_1 = \frac{1}{L}\int_0^{Lt_{MCD}} Nu_1\, dL = \frac{1}{L}\left(-0.84\, Pr_b^{-0.2} Lt_{MCD} + 0.72(Re_b D)^{0.54} Pr_b^{0.34} Lt_{MCD}^{0.46}\right)$$

$$\overline{Nu}_2 = \frac{1}{L}\int_{Lt_{MCD}}^{L} Nu_2\, dL = \frac{1}{L}\left(0.207Gr_b^{0.305} - 1.19\right)Pr_b^{0.42}(Re_b D)^{-0.08}(L - Lt_{MCD})$$

$$Lt_{MCD} = \frac{2.4Re_b Pr_b^{0.6} D}{Gr_b^{0.57}} \text{ for } L > Lt_{MCD} \text{ and } Lt_{MCD} = L \text{ for } L < Lt_{MCD}$$

In this equation, as well as Eq. (33), the Reynolds numbers, Prandtl numbers and Grashof numbers are evaluated at the bulk fluid temperature. Similarly, Eq. (33) was developed to calculate the Nusselt numbers as a function of the modified Grashof number:

$$\overline{Nu} = 4.36 + \overline{Nu}_1 + \overline{Nu}_2 \quad (33)$$

$$\overline{Nu}_1 = \frac{1}{L}\int_0^{Lt_{MCD}} Nu_1\, dL = \frac{1}{L}(-0.84\, Pr_b^{-0.2} Lt_{MCD} + 0.72(Re_b D)^{0.54} Pr_b^{0.34} Lt_{MCD}^{0.46})$$

$$\overline{Nu}_2 = \frac{1}{L}\int_{Lt_{MCD}}^{L} Nu_2\, dL = \frac{1}{L}\left(0.202Gr_b^{*\,0.254} - 1.23\right)Pr_b^{0.39}(Re_b D)^{-0.06}(L - Lt_{MCD})$$

$$Lt_{MCD} = \frac{2.1Re_b Pr_b^{0.6} D}{Gr_b^{*\,0.45}} \text{ for } L > Lt_{MCD} \text{ and } Lt_{MCD} = L \text{ for } L < Lt_{MCD}$$

In the transitional flow regime, the heat transfer characteristics are a function of both free convection effects and Prandtl number, therefore the following Nusselt number correlation was developed by Meyer *et al*. [32]:

$$\overline{Nu} = (0.017Re_b - 30.3)Gr_b^{-0.08} Pr_b^{0.33} \quad (34)$$

Meyer *et al*. [32] also developed the following correlation for quasi-turbulent and turbulent flow:

$$Nu = 0.058(Re - 500)^{1.07} Pr^{0.42} \left(\frac{Pr}{Pr_s}\right)^{0.11} f \quad (35)$$

This correlation is valid for a very wide range of Reynolds numbers and Prandtl numbers. Similar to Friend and Metzner [68], $Pr^{0.42}$ was used to account for different Prandtl number fluids, while $(Pr/Pr_s)^{0.11}$ was used to account for variable fluid properties across the cross-section [69]. Due to the very strong relationship between pressure drop and heat transfer, the Blasius friction factor [70] was incorporated. It was decided to use the Blasius friction factor, because friction factor data might not necessarily be available and Meyer *et al*. [32] concluded that the Blasius correlation is both accurate and simple. Gnielinski [69] found that better correlation was obtained at lower Reynolds numbers close to the transitional flow regime when the heat transfer results were plotted as a function of (*Re*-1 000). However, Meyer *et al*. [32] found that best results were obtained when the heat transfer results were plotted in terms of $Nu/[Pr^{0.42}(Pr/Pr_w)^{0.11}]f$ as a function of $(Re - 500)$. It was also noted that Eq. (35) will most probably be valid for rough tubes if the friction factors of the rough tube can be determined.

By substituting the friction factor with the Blasius correlation ($f = 0.3125Re^{-0.25}$), the following Nusselt number for quasi-turbulent and turbulent flow was obtained [32]:

$$Nu = 0.018Re^{-0.25}(Re - 500)^{1.07} Pr^{0.42} \left(\frac{Pr}{Pr_w}\right)^{0.11} \quad (36)$$

Because the heat transfer coefficients of developing flow are higher than for fully developed flow, Gnielinski [69] used the term $[1 + (D/L)^{2/3}]$ to account for very short tubes. Meyer *et al*. [32] found that the same term $[1 + (D/L)^{2/3}]$ can be added to Eq. (36). This led to the following general correlation to calculate the Nusselt numbers of quasi-turbulent and turbulent flow in short tubes:

$$Nu = 0.018Re^{-0.25}(Re - 500)^{1.07} Pr^{0.42} \left(\frac{Pr}{Pr_w}\right)^{0.11} \left[1 + \left(\frac{D}{L}\right)^{2/3}\right] \quad (37)$$

By making use of the method of Churchill and Usagi [71], Meyer *et al*. [32] proposed a single correlation that is valid for all flow regimes:

$$\overline{Nu} = \left[\overline{Nu}_{Eq.(32)}^{10} + \left(\overline{Nu}_{Eq.(34)}^{-8} + \overline{Nu}_{Eq.(36)}^{-8}\right)^{-10/8}\right]^{0.1} \quad (38)$$

Eq. (32) (laminar flow), Eq. (34) (transitional flow) and Eq. (36) (quasi-turbulent and turbulent flow) should be used to calculate $Nu_{Eq.(32)}$, $Nu_{Eq.(34)}$, and $Nu_{Eq.(36)}$ respectively, in terms of the Grashof number.

Furthermore, Meyer *et al*. [32] noted that the following correlation can be extracted from Eq. (38) to obtain a single correlation that is valid for transitional to turbulent flow:

$$\overline{Nu} = \left(\overline{Nu}_{Eq.(34)}^{-8} + \overline{Nu}_{Eq.(36)}^{-8}\right)^{-1/8} \quad (39)$$

where Eq. (34) (transitional flow) and Eq. (36) (quasi-turbulent and turbulent flow) should be used to calculate $Nu_{Eq.(34)}$, and $Nu_{Eq.(36)}$, respectively.

Table 5: Overall performance and ranges of the local laminar Nusselt number correlations. The value of *n* represents the number of data points and Ave %, the average deviation [31].

	Eq.	Range	Data points	±10% [%]	±20% [%]	Ave [%]
Local						
$Nu = 4.36 + (Nu_1^6 + Nu_2^6)^{1/6}$ $Nu_1 = (0.33Gz^{0.54} - 0.84)Pr^{-0.2}$ $Nu_2 = (0.207Gr^{0.305} - 1.19)Pr^{0.5}Gz^{-0.08}$	(30)	467 ≤ *Re* ≤ 3 217, 3 ≤ *Pr* ≤ 7.4, 2.6 ≤ *Gz* ≤ 5 589, 30 ≤ *Gr* ≤ 2.49×10^5, 541 ≤ *Gr** ≤ 4.01×10^6	5 680	87	99	5.4
$Nu = 4.36 + (Nu_1^6 + Nu_2^6)^{1/6}$ $Nu_1 = (0.33Gz^{0.54} - 0.84)Pr^{-0.2}$ $Nu_2 = (0.202Gr^{*\,0.254} - 1.23)Pr^{0.45}Gz^{-0.06}$	(31)		5 680	89	99	5.3
Average						
$Nu = 4.36 + Nu_1 + Nu_2$ $Nu_1 = \frac{1}{L}(-0.84\ Pr^{-0.2}Lt_{MCD} + 0.72(ReD)^{0.54}Pr^{0.34}Lt_{MCD}^{0.46})$ $Nu_2 = \frac{1}{L}(0.207Gr^{0.305} - 1.19)Pr^{0.42}(ReD)^{-0.08}(L - Lt_{MCD})$ $Lt_{MCD} = \frac{2.4RePr^{0.6}D}{Gr^{0.57}}$ for *L* > *Lt*$_{MCD}$ and *Lt*$_{MCD}$ = *L* for *L* < *Lt*$_{MCD}$	(32)	48 ≤ *Re* ≤ 3 217, 2.9 ≤ *Pr* ≤ 282, 2.6 ≤ *Gz* ≤ 1.14×10^5, 5.5 ≤ *Gr* ≤ 4.51×10^5	495	98	100	3.6
$\overline{Nu} = 4.36 + \overline{Nu}_1 + \overline{Nu}_2$ $\overline{Nu}_1 = \frac{1}{L}(-0.84\ Pr_b^{-0.2}Lt_{MCD} + 0.72(Re_bD)^{0.54}Pr_b^{0.34}Lt_{MCD}^{0.46})$ $\overline{Nu}_2 = \frac{1}{L}(0.202Gr_b^{*\,0.254} - 1.23)Pr_b^{0.39}(Re_bD)^{-0.06}(L - Lt_{MCD})$ $Lt_{MCD} = \frac{2.1Re_bPr_b^{0.6}D}{Gr_b^{*\,0.45}}$ for *L* > *Lt*$_{MCD}$ and *Lt*$_{MCD}$ = *L* for *L* < *Lt*$_{MCD}$	(33)		495	95	100	3.6

Table 6: Summary of the ranges and performance of the average transitional, quasi-turbulent and turbulent Nusselt number correlations.

	Eq.	Range	Data points	±10% [%]	±20% [%]	Ave [%]
Transitional $Nu = (0.017Re - 30.3)Pr^{0.33}Gr^{-0.08}$	(34)	2 115 ≤ *Re* ≤ 3 586, 4 ≤ *Pr* ≤ 49, $1.19\times10^3 \leq Gr \leq 1.75\times10^5$	119 101*	43 46	70 73	15 14
Quasi-turbulent and turbulent $Nu = 0.058(Re - 500)^{1.07}Pr^{0.42}\left(\frac{Pr}{Pr_w}\right)^{0.11} f$ **	(35)	2 445 < *Re* < 401 600 0.5 < *Pr* < 276 $0.85 < (Pr/Pr_w)^{0.11} < 1.17$	2 351 1 180*	72 95	88 100	9.5 4.4
$Nu = 0.018Re^{-0.25}(Re - 500)^{1.07}Pr^{0.42}\left(\frac{Pr}{Pr_w}\right)^{0.11}$	(36)					
Quasi-turbulent and turbulent (Short tubes) $Nu = 0.018Re^{-0.25}(Re - 500)^{1.07}Pr^{0.42}\left(\frac{Pr}{Pr_w}\right)^{0.11}\left[1 + \left(\frac{D}{L}\right)^{2/3}\right]$	(37)	2 445 < *Re* < 401 600 0.5 < *Pr* < 276 $1.0081 < [1 + (D/L)^{2/3}] < 1.15$ $0.85 < (Pr/Pr_w)^{0.11} < 1.17$	2 351 1 180*	73 95	88 100	9.8 4.4
Transitional, quasi-turbulent and turbulent $Nu = \left(Nu_{Eq.(34)}^{-8} + Nu_{Eq.(36)}^{-8}\right)^{-1/8}$	(39)	2 282 ≤ *Re* ≤ 46 001, 4 ≤ *Pr* ≤ 49, $334 \leq Gr \leq 1.75\times10^5$ $1.0 < (Pr/Pr_w)^{0.11} < 1.02$	584 542*	64 63	90 89	9.3 9.5
All flow regimes $Nu = \left[Nu_{Eq.(32)}^{10} + \left(Nu_{Eq.(34)}^{-8} + Nu_{Eq.(36)}^{-8}\right)^{-10/8}\right]^{0.1}$	(38)	597 ≤ *Re* ≤ 46 001, 3 ≤ *Pr* ≤ 139, $334 \leq Gr \leq 4.04\times10^5$	837 768*	60 60	79 79	18 18

Notes: *Performance evaluated using the experimental data of Meyer *et al*. [32]; **Suitable for rough tubes when appropriate friction factor is used

Table 5 summarises the ranges and performance of the local and average laminar correlations. The local correlations were able to predict all the data within 20%, while the average correlations could predict all the data within 20%. The validity/accuracy of Eqs. (30) and (31) for Prandtl numbers less than one was determined using 34 experimental data points obtained using air at $Re \approx 740$, $Pr \approx 0.7$ and $3.34 < Gr < 491$. It was found that Eq. (30) could predict 71% of the data within 20% and the average deviation was 15%, while Eq. (31) could predict 80% of the data within 20% and the average deviation was 13%. Table 6 summarises the valid ranges and performances of the average Nusselt number correlations for developing and fully developed transitional, quasi-turbulent and turbulent flow.

9. Flow Regime Maps

Everts and Meyer [26] found that there were no suitable criteria or flow regime map in literature to accurately predict the convection flow regime of the experimental data obtained using low Prandtl number fluids in tubes with relatively small diameters and a constant heat flux boundary condition. New easy-to-use flow regime maps for developing and fully developed flow using different test fluids and tube diameters were therefore developed. These flow regime maps are unique for four reasons. Firstly, they contain contour lines that show the Nusselt number enhancements due to the free convection effects. Secondly, they are valid for a wide range of tube diameters and Prandtl numbers. Thirdly, the flow regime maps are developed as a function of temperature difference (Grashof number) and heat flux (modified Grashof number). Finally, four of the six flow regime maps are not only valid for fully developed flow, but also for developing flow.

9.1. Forced/mixed convection boundary

Metais and Eckert [72] defined the boundary between forced and mixed convection as the location where the heat transfer coefficients are 10% greater than the corresponding forced convection case ($Nu/Nu_{FC} > 1.1$), while Tam *et al*. [11] defined it as the location where h_t/h_b decreases below 0.8. These two criteria are compared in Fig. 14 by dividing the fully developed laminar Nusselt numbers by 4.36 (fully developed forced convection laminar flow) and plotting the results against h_t/h_b. The dotted black and green lines represent the criteria of Metais and Eckert [72] and Tam *et al*. [11], respectively.

For low Prandtl number fluids such as water, Fig. 14 indicates that the values of Nu/Nu_{FC} were significantly affected by tube diameter and it increased from one to approximately four that as the tube diameter was increased from 4 mm to 19 mm. This was as expected, because free convection effects increase with increasing tube diameter ($Gr \propto D^3$). However, there was only a slight decrease in h_t/h_b and it did not decrease below 0.8 in the 11.5 mm and 19 mm test sections. Although Nu/Nu_{FC} of the results of Strickland [65], who used pure ethylene glycol in a 15.8 mm test section, was approximately between the results of the 11.5 mm and 19 mm test sections, h_t/h_b was significantly lower. This is due to the increased circumferential and axial temperature differences, which are caused by the low thermal conductivity and specific heat, as well as the high viscosity of ethylene glycol.

As expected, the values of h_t/h_b in the 19 mm test section were less than in the 11.5 mm test section; however, the minimum h_t/h_b-value in the 4 mm test section was less than in the 11.5 mm and 19 mm test sections. There is thus no distinct trend between h_t/h_b and tube diameter. Fig. 14 also indicates that h_t/h_b is very dependent on the fluid properties and differs significantly when the results of different test fluids, for example, water and ethylene glycol, are compared. Furthermore, the heat transfer coefficient ratio criterion, $h_t/h_b < 0.8$, is too conservative for low Prandtl number fluids such

as water. At h_t/h_b = 0.8, Nu/Nu_{FC} in the 4 mm test section ranged between 1.16 and 1.4, which means that the Nusselt numbers were between 16% and 40% greater than the corresponding forced convection case. Furthermore, h_t/h_b in the 11.5 mm test section did not decrease below 0.83, while Nu/Nu_{FC} varied between 1.9 and 2.9. Everts and Meyer [26] therefore concluded that $h_t/h_b \leq 0.95$ is more appropriate for low Prandtl number fluids such as water, because this corresponded to the point where Nu/Nu_{FC} exceeded 1.1 in the 4 mm test section.

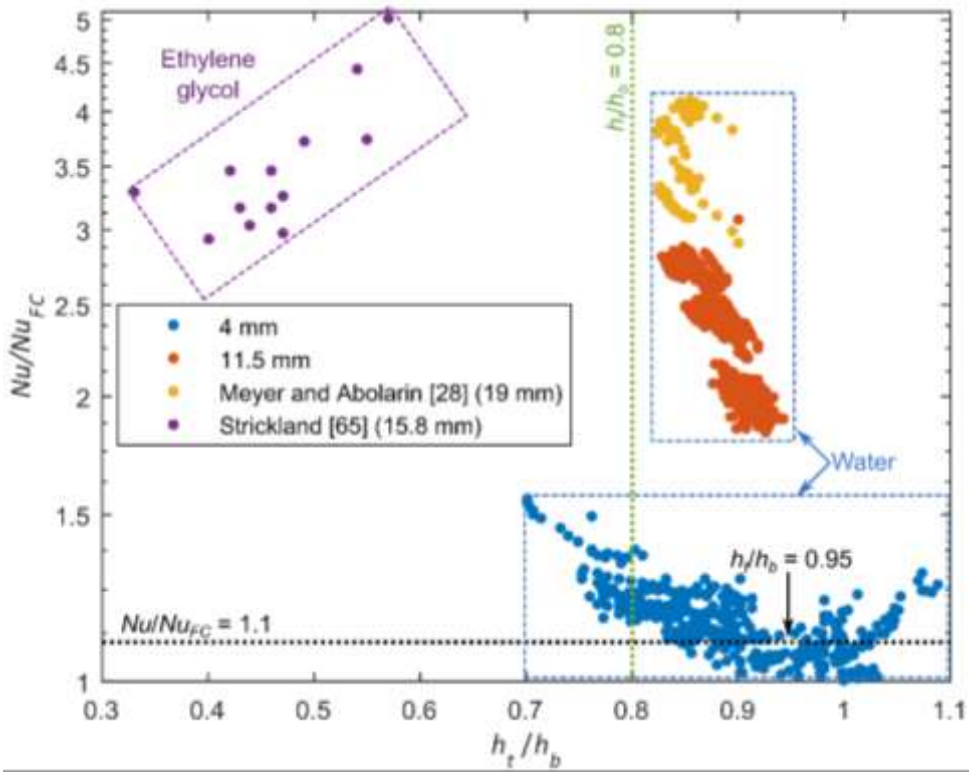

Fig. 14: Comparison of the experimental data of this study and literature [28, 65] in terms of Nu/Nu_{FC} (where Nu_{FC} = 4.36) against h_t/h_b at different constant heat fluxes for different tube diameters and test fluids [26].

Although h_t/h_b is an appropriate criterion for the high Prandtl number fluids, such as the data of Strickland [65], the 10% increase in heat transfer coefficient criterion, $Nu/Nu_{FC} > 1.1$, is more suitable for low Prandtl number fluids, because it increases with increasing tube diameter and heat flux, which is known to increase free convection effects. Although h_t/h_b is a valuable tool to gain insight into the local free convection effects along the test section and how they are influenced by Reynolds number and heat flux, care should be taken when different tube diameters and especially test fluids are compared, because it significantly affects the values of h_t/h_b.

9.2. Flow regime map for fully developed flow

Figures 15 and 16 are the flow regime maps of Everts and Meyer [26] for fully developed flow in terms of *Ra* and *Ra**, respectively. As these flow regime maps are for fully developed flow, Nu_{FC} = 4.36 for all data below the Re_{cr}-line (Eqs. (40) and (44)), while Nu_{FC} is the corresponding forced convection Nusselt number from general literature for all data above the Re_{qt}-line (Eqs. (41) and (45)). In the transitional flow regime ($Re_{cr} < Re < Re_{qt}$, thus all the data between Eqs. (40) and (41), and Eqs. (44) and (45)), no correlations could be found in literature for both forced convection and mixed convection conditons. Therefore, Nu/Nu_{FC} only gives an estimate (as it was not based on measurements, but obtained through a curve fit) of whether free convection effects can be expected or not, and not the actual Nusselt number values.

As indicated by the dotted lines in Fig. 15 and Fig. 16, $Ra < 4\,970$ and $Ra^* < 2.40\times10^4$ can be used as Reynolds number independent criteria ($Nu/Nu_{FC} = 1.1$), which will ensure that the flow regime will most probably be forced convection. More conservative criteria ($Nu/Nu_{FC} = 1$) will be $Ra < 2\,520$ and $Ra^* < 1.02\times10^4$.

The equations of the transitional flow regime boundaries and the forced/mixed convection boundaries of the flow regime maps in Fig. 15 and Fig. 16 (for fully developed flow) are summarised in Table 7. Proposed average Nusselt number correlations are also included in these flow regime maps (as well as for the flow regime maps for developing flow in Section 9.3). However, it should be noted that Everts and Meyer [26] developed these correlations using water data only, while the flow regime maps are valid for high Prandtl number fluids as well. Therefore, other suitable Nusselt number correlations (for different test fluids) can be used in combination with these flow regime maps.

Table 7: Equations of the transitional flow regime boundaries and forced/mixed convection boundaries, as well as the ranges of the flow regime maps as a function of *Ra* and *Ra [26].**

		Correlation	Eq.
Ra (Fig. 15)	Re_{cr}	$Re_{cr} = 1272\,Ra^{0.06834}$	(40)
	Re_{qt}	$Re_{qt} = 2846\,Ra^{0.02177}$	(41)
	$Re < Re_{cr}$	$FC/MC = 7.278\times10^{7}\,Ra^{-1.212} - 202.3$	(42)
	$Re_{cr} < Re < Re_{qt}$	$FC/MC = -1.123\times10^{5}\,Ra^{-0.4958} + 3950$	(43)
*Ra** (Fig. 16)	Re_{cr}	$Re_{cr} = 1730.9\,Ra^{*\,0.0549}$	(44)
	Re_{qt}	$Re_{qt} = 3056.4\,Ra^{*\,0.0217}$	(45)
	$Re < Re_{cr}$	$FC/MC = 2.73\times10^{9}\,Ra^{*\,-1.39} + 75.5$	(46)
	$Re_{cr} < Re < Re_{qt}$	$FC/MC = -3.338\times10^{4}\,Ra^{*\,-0.3112} + 3839$	(47)
Ranges		$546 \le Re \le 11\,247$, $3 \le Pr \le 139.4$, $26 \le Gr \le 4.2\times10^5$, $561 \le Gr^* \le 7\times10^6$	

Everts and Meyer [26] evaluated the performance of the flow regime maps in Fig. 15 and Fig. 16 in the laminar flow regime by comparing $Nu/4.36$ of their experimental data with the Nu/Nu_{FC} values in the flow regime maps, and the results are summarised in Table 8. Both flow regime maps could predict approximately all their experimental data, as well as experimental data from literature [28, 65], within 10%. It should therefore be possible to use these flow regime maps as reliable tools to predict the convection flow regime of fully developed flow in a wide range of tube diameters and Prandtl numbers.

Table 8: Ranges and performance of the flow regime maps in Fig. 15 and Fig. 16 [26].

	Everts and Meyer [26]				Everts and Meyer [26] and literature [28, 65]			
Range	$546 \le Re \le 2\,936$, $3 \le Pr \le 6.5$, $26 \le Gr \le 9.4\times10^4$, $610 \le Gr^* \le 1.2\times10^6$				$546 \le Re \le 2\,936$, $3 \le Pr \le 139.4$, $26 \le Gr \le 4.2\times10^5$, $561 \le Gr^* \le 7\times10^6$			
	n	±10% [%]	±20% [%]	Ave %	*n*	±10% [%]	±20% [%]	Ave %
Ra: Fig. 15	917	97	100	3.4	985	95	99.7	3.6
*Ra**: Fig. 16	916	99	100	2.8	984	98	100	3.0

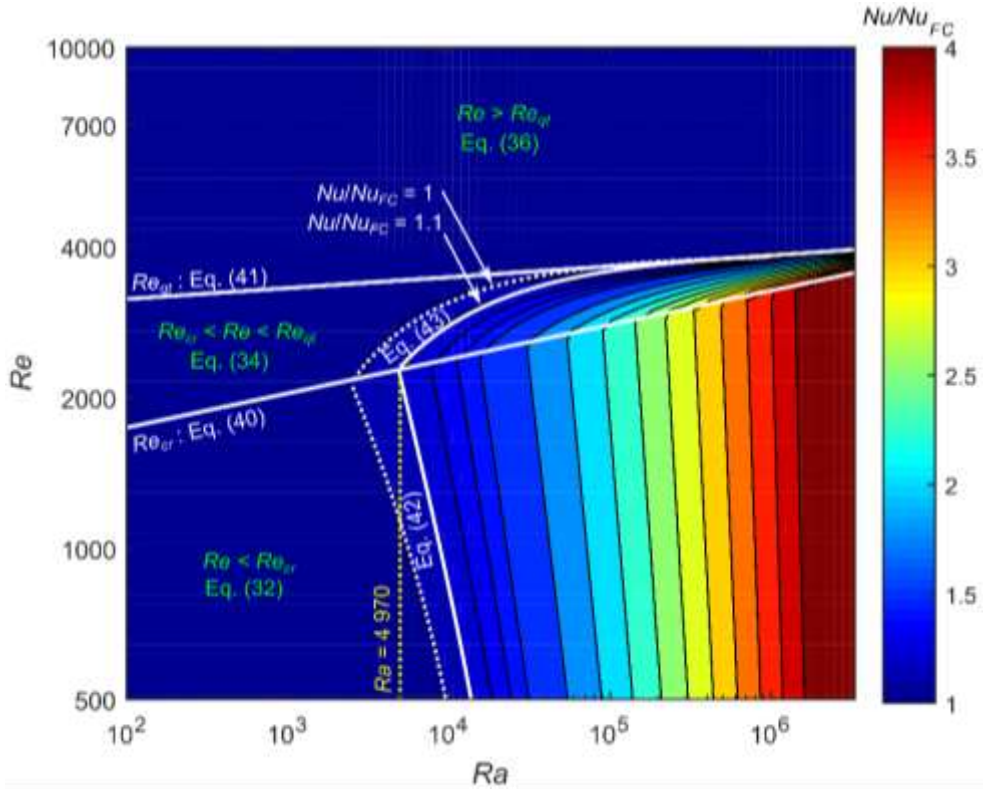

Fig. 15: Flow regime map for fully developed flow as a function of *Re* and *Ra*. Nu_{FC} = 4.36 for all data below Eq. (40), while Nu_{FC} is the corresponding forced convection Nusselt number from general literature for all data above Eq. (41). In the transitional flow regime ($Re_{cr} < Re < Re_{qt}$), Nu/Nu_{FC} only gives an estimate of whether free convection effects can be expected or not, and not the actual Nusselt number values [26].

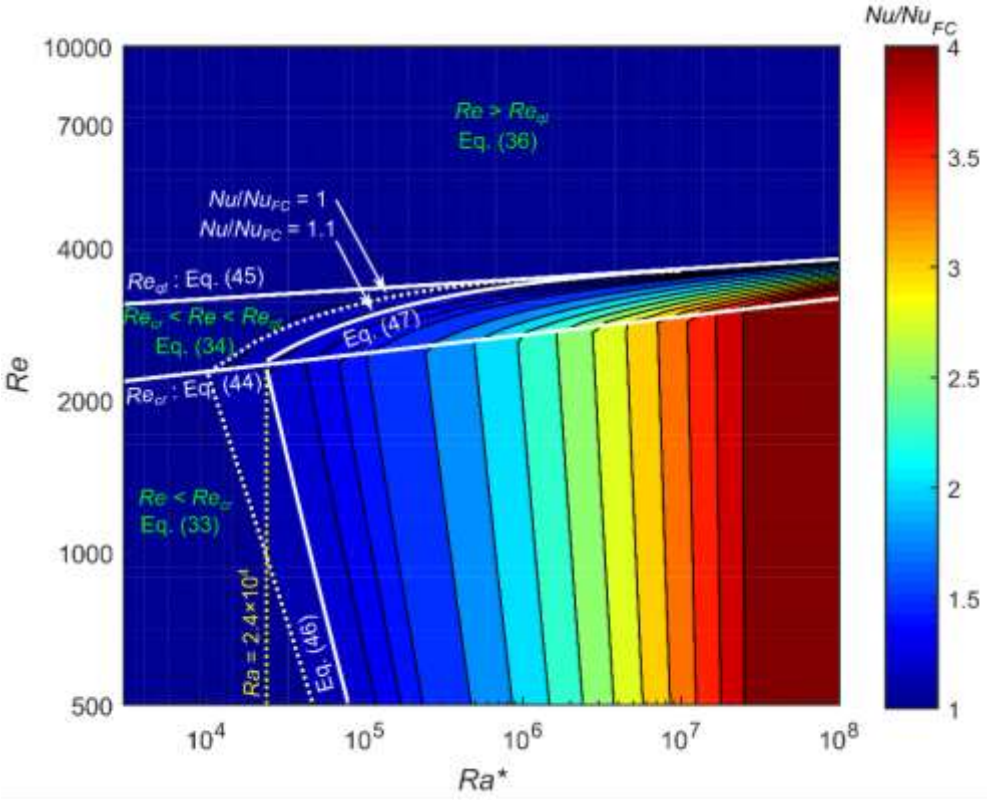

Fig. 16: Flow regime map for fully developed flow as a function of *Re* and *Ra. Nu_{FC} = 4.36 for all data below Eq. (44), while Nu_{FC} is the corresponding forced convection Nusselt number for all data above Eq. (45). In the transitional flow regime ($Re_{cr} < Re < Re_{qt}$), Nu/Nu_{FC} only gives an estimate of whether free convection effects can be expected or not, and not the actual Nusselt number values [26].**

9.3. Flow regime map for developing flow

Everts and Meyer [26] developed the first flow regime maps for developing flow. Figures 17 and 18 contains the flow regime maps in terms of $Ri(x/D)$ and Ra/Gz, respectively. In both flow regime maps, $Nu_{FC} = Nu_{SL}$ for all data below the Re_{cr}-lines (Eqs. (49) and (53)), while Nu_{FC} is the corresponding forced convection Nusselt number from general literature for all data above the Re_{qt}-lines (Eqs. (50) and (54)). The correlation of Shah and London [60] (Eq. (48)) was used as the laminar forced convection reference Nusselt number, because a constant heat flux boundary condition was used and the flow was simultaneously hydrodynamically and thermally developing:

$$Nu_{SL} = Nu_1 \times Nu_2 - 1 \tag{48}$$

where

$$Nu_1 = \left[1 + \left(\frac{\pi/(115.2\ z^*)}{\{1 + (Pr/0.0207)^{2/3}\}^{1/2}\ \{1 + (220\ z^*/\pi)^{-10/9}\}^{3/5}}\right)^{5/3}\right]^{3/10}$$

$$Nu_2 = 5.364\left[1 + (220\ z^*/\pi)^{-10/9}\right]^{3/10}$$

$$z^* = \frac{\pi}{4Gz}$$

It should be noted that the values of Nu_{FC} given in the rest of this section are not only a function of Reynolds number and Prandtl number, but most importantly, a function of axial position, as the flow is developing. In the transitional flow regime ($Re_{cr} < Re < Re_{qt}$), Nu/Nu_{FC} only gives an estimate of whether free convection effects can be expected or not, and not the actual Nusselt number values.

The yellow dotted lines in Fig. 17 and Fig. 18 indicate that $Ri(x/D) < 0.21$ and $Ra/Gz < 518$ can be used as Reynolds number independent criteria ($Nu/Nu_{FC} = 1.1$), which will ensure that the flow will most probably be forced convection. More conservative criteria ($Nu/Nu_{FC} = 1$) will be $Ri(x/D) < 0.14$ and $Ra/Gz < 318$. The equations of the transitional flow regime boundaries and the forced/mixed convection boundaries are summarised in Table 9, while the performance of the flow regime maps is summarised in Table 11.

Table 9: Equations of the transitional flow regime boundaries and forced/mixed convection boundaries, as well as the ranges of the flow regime maps as a function of $Ri(x/D)$ and Ra/Gz [26].

		Correlation	Eq.
$Ri(x/D)$ (Fig. 17)	Re_{cr}	$Re_{cr} = 2675.3\left(Ri(x/D)\right)^{0.0532}$	(49)
	Re_{qt}	$Re_{qt} = 3595.1\left(Ri(x/D)\right)^{0.0216}$	(50)
	$Re < Re_{cr}$	$FC/MC = 546.3\left(Ri(x/D)\right)^{-0.9212} + 145.7$	(51)
	$Re_{cr} < Re < Re_{qt}$	$FC/MC = -540.8\left(Ri(x/D)\right)^{-0.5939} + 3896$	(52)
Ra/Gz (Fig. 18)	Re_{cr}	$Re_{cr} = 1730.9(Ra/Gz)^{0.0549}$	(53)
	Re_{qt}	$Re_{qt} = 3056.4(Ra/Gz)^{0.0217}$	(54)
	$Re < Re_{cr}$	$FC/MC = 6.591 \times 10^{16}(Ra/Gz)^{-4.944} - 50.47$	(55)
	$Re_{cr} < Re < Re_{qt}$	$FC/MC = -3.582 \times 10^{4}(Ra/Gz)^{-0.512} + 3984$	(56)
	Ranges	$502 \le Re \le 11\,247$, $3 \le Pr \le 139.4$, $2.7 \le Gz \le 5.5\times10^3$, $26 \le Gr \le 4.2\times10^5$, $561 \le Gr^* \le 7\times10^6$	

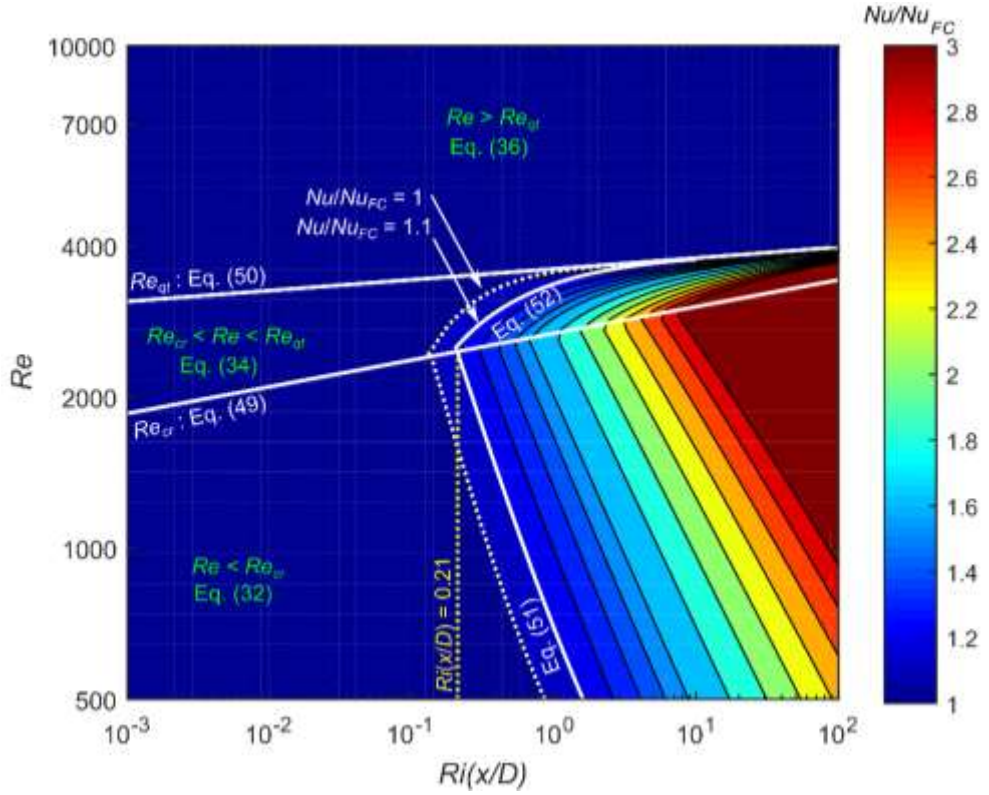

Fig. 17: Flow regime map for developing and fully developed flow as a function of *Re* and *Ri*(*x*/*D*). $Nu_{FC} = Nu_{SL}$ for all data below Eq. (49), while Nu_{FC} is the corresponding forced convection Nusselt number from general literature for all data above Eq. (50). In the transitional flow regime ($Re_{cr} < Re < Re_{qt}$), Nu/Nu_{FC} only gives an estimate of whether free convection effects can be expected or not, and not the actual Nusselt number values [26].

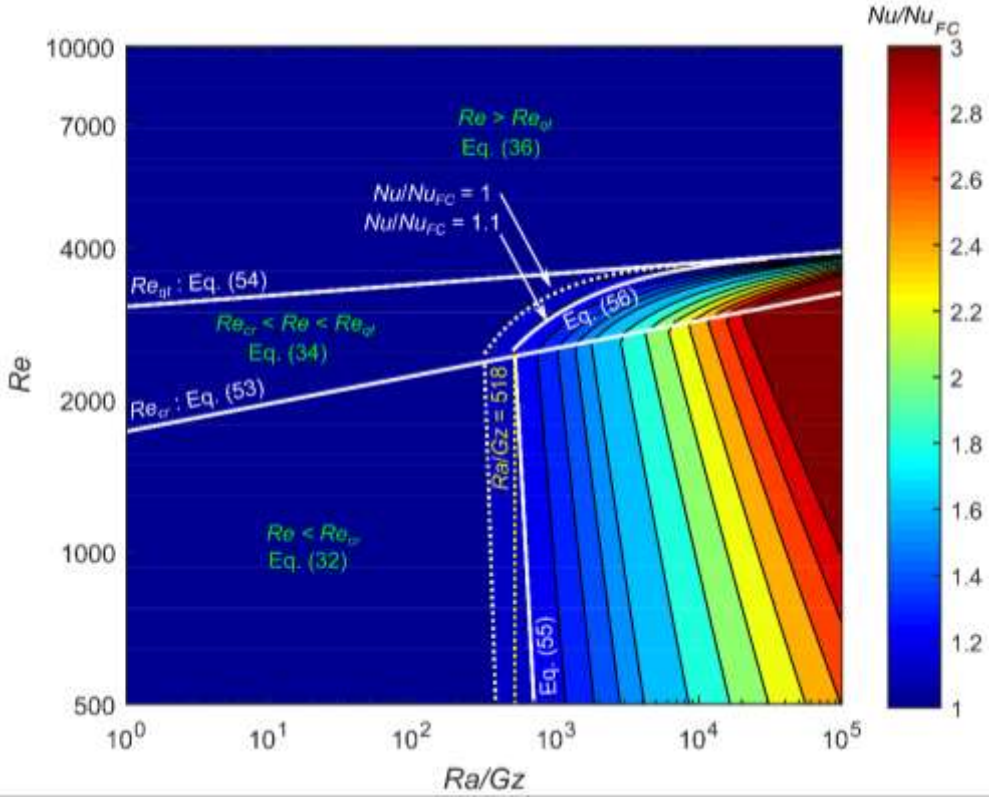

Fig. 18: Flow regime map for developing and fully developed flow as a function of *Re* and *Ra*/*Gz*. $Nu_{FC} = Nu_{SL}$ for all data below Eq. (53), while Nu_{FC} is the corresponding forced convection Nusselt number from general literature for all data above Eq. (54). In the transitional flow regime ($Re_{cr} < Re < Re_{qt}$), Nu/Nu_{FC} only gives an estimate of whether free convection effects can be expected or not, and not the actual Nusselt number values [26].

Furthermore, Everts and Meyer [26] developed flow regime maps for developing flow in terms of the modified Grashof, Rayleigh and Richardson numbers, because the temperature difference (required to calculate the Grashof number for constant heat flux problems) is not always available while the heat flux usually is. Figures 19 and 20 contain the flow regime maps in terms of $Ri^*(x/D)$ and Ra^*/Gz respectively. In both flow regime maps, $Nu_{FC} = Nu_{SL}$ for all data below the Re_{cr}-line (Eqs. (57) and (61)), while Nu_{FC} is the corresponding forced convection Nusselt number from general literature for all data above the Re_{qt}-line (Eqs. (58) and (62)). In the transitional flow regime ($Re_{cr} < Re < Re_{qt}$), Nu/Nu_{FC} only gives an estimate of whether free convection effects can be expected or not, and not the actual Nusselt numbers. The yellow dotted lines in Fig. 19 and Fig. 20 indicate that $Ri^*(x/D) < 1.64$ and $Ra^*/Gz < 4\,038$ can be used as Reynolds number independent criteria ($Nu/Nu_{FC} = 1.1$), which will ensure that the flow regime will most probably be forced convection. More conservative criteria ($Nu/Nu_{FC} = 1$) will be $Ri^*(x/D) < 1$ and $Ra^*/Gz < 2\,364$.

Table 10 summarises the equations of the transitional flow regime boundaries and forced/mixed convection boundaries, and the performance of flow regime maps for developing flow is summarised in Table 11. The performance was determined by comparing Nu/Nu_{SL} of the experimental data and the Nu/Nu_{FC} values in the flow regime maps in Fig. 17 to Fig. 20. Table 11 indicates that all four flow regime maps could predict approximately 80% of the data within 10%, and almost all the data within 20%. The two flow regime maps (Fig. 19 and Fig. 20) which are a function of heat flux (Gr^*) performed slightly better than the flow regime maps (Fig. 17 and Fig. 18) which are a function of temperature difference (Gr).

Table 10: Equations of the transitional flow regime boundaries and forced/mixed convection boundaries, as well as the ranges of the flow regime maps as a function of $Ri^*(x/D)$ and Ra^*/Gz[26].

		Correlation	Eq.
$Ri^*(x/D)$ (Fig. 19)	Re_{cr}	$Re_{cr} = 2355.5\left(Ri^*(x/D)\right)^{0.0567}$	(57)
	Re_{qt}	$Re_{qt} = 3377.3\left(Ri^*(x/D)\right)^{0.0195}$	(58)
	$Re < Re_{cr}$	$FC/MC = 3724\left(Ri^*(x/D)\right)^{-0.7711} + 115.4$	(59)
	$Re_{cr} < Re < Re_{qt}$	$FC/MC = -1868\left(Ri^*(x/D)\right)^{-0.6159} + 3772$	(60)
Ra^*/Gz (Fig. 20)	Re_{cr}	$Re_{cr} = 1401.3(Ra^*/Gz)^{0.0635}$	(61)
	Re_{qt}	$Re_{qt} = 2820.8(Ra^*/Gz)^{0.0215}$	(62)
	$Re < Re_{cr}$	$FC/MC = 5.8 \times 10^{22}(Ra^*/Gz)^{-5.373}$	(63)
	$Re_{cr} < Re < Re_{qt}$	$FC/MC = -1.224 \times 10^{4}(Ra^*/Gz)^{-0.543} + 3787$	(64)
	Ranges	$502 \le Re \le 11\,247$, $3 \le Pr \le 139.4$, $2.7 \le Gz \le 5.5\times10^{3}$, $26 \le Gr \le 4.2\times10^{5}$, $561 \le Gr^* \le 7\times10^{6}$	

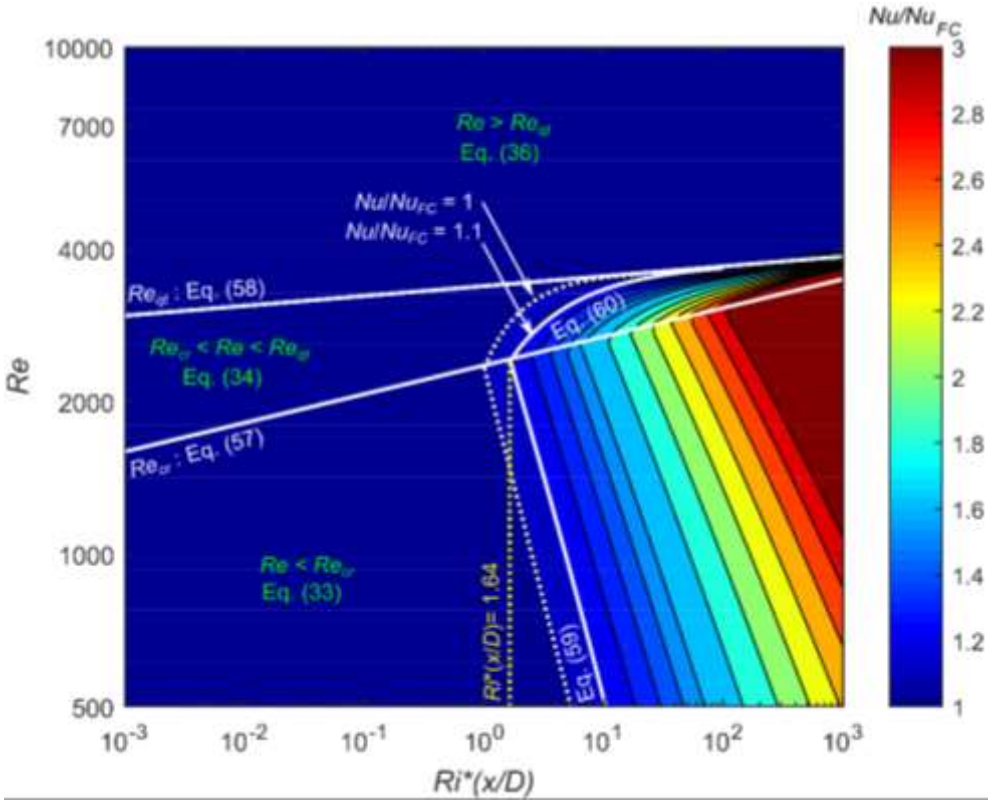

Fig. 19: Flow regime map for developing and fully developed flow as a function of *Re* and *Ri*(x/D)*. $Nu_{FC} = Nu_{SL}$ for all data below Eq. (57), while Nu_{FC} is the corresponding forced convection Nusselt number from general literature for all data above Eq. (58). In the transitional flow regime ($Re_{cr} < Re < Re_{qt}$), Nu/Nu_{FC} only gives an indication of whether free convection effects can be expected or not, and not the actual Nusselt number values [26].

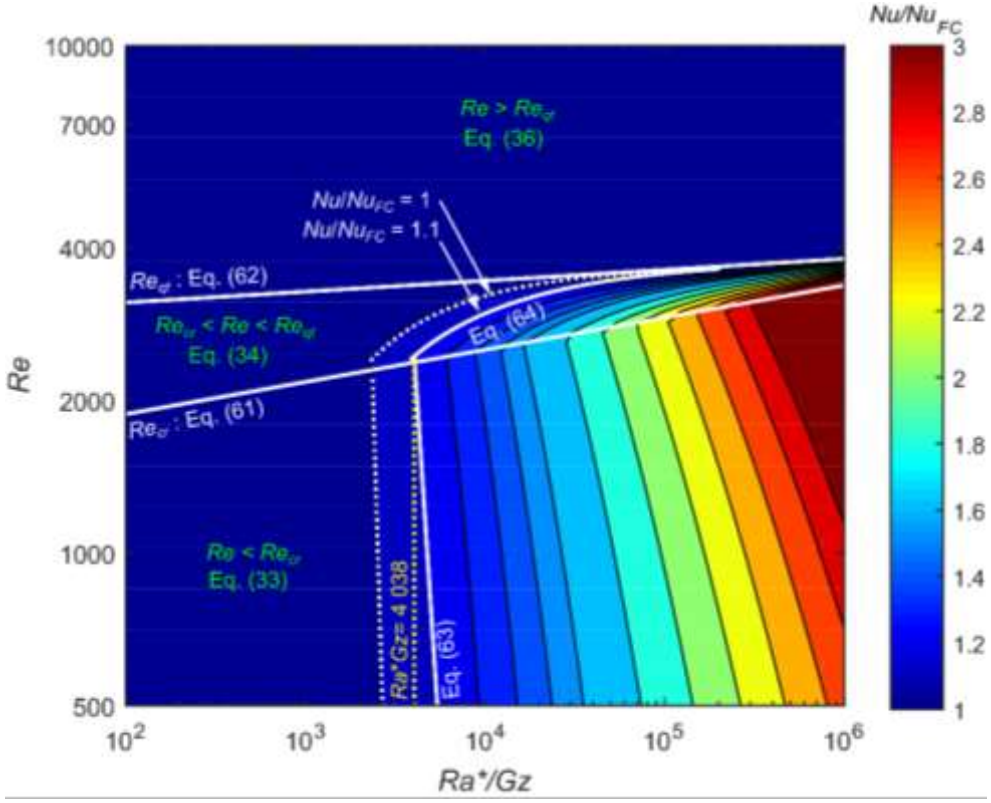

Fig. 20: Flow regime map for developing and fully developed flow as a function of *Re* and *Ra*/Gz*. $Nu_{FC} = Nu_{SL}$ for all data below Eq. (61), while Nu_{FC} is the corresponding forced convection Nusselt number from general literature for all data above Eq. (62). In the transitional flow regime ($Re_{cr} < Re < Re_{qt}$), Nu/Nu_{FC} only gives an indication of whether free convection effects can be expected or not, and not the actual Nusselt number values [26].

Table 11: Ranges and performance of the flow regime maps in Fig. 17 to Fig. 20 using developing and fully developed data [26].

	Everts and Meyer [26]				Everts and Meyer [26] and literature [28, 65]			
Range	502 ≤ Re ≤ 2 936, 3 ≤ Pr ≤ 6.9, 2.7 ≤ Gz ≤ 689, 106 ≤ Gr ≤ 9.4×10^4, 569 ≤ Gr^* ≤ 1.2×10^6				502 ≤ Re ≤ 2 936, 3 ≤ Pr ≤ 139.5, 2.7 ≤ Gz ≤ 1 241, 106 ≤ Gr ≤ 4.2×10^5, 569 ≤ Gr^* ≤ 7.0×10^6			
	n	±10% [%]	±20% [%]	Ave %	n	±10% [%]	±20% [%]	Ave %
$Ri(x/D)$: Fig. 17	1 776	77	97	6.7	2 174	79	95	6.6
Ra/Gz: Fig. 18	1 776	78	97	6.7	2 152	80	95	6.6
$Ri^*(x/D)$: Fig. 19	1 777	82	99	5.7	2 159	84	96	5.9
Ra^*/Gz: Fig. 20	1 747	83	99	5.7	2 085	84	96	5.9

To determine the validity/accuracy of the flow regime maps for Prandtl numbers less than one, the performance of the flow regime maps was determined using experimental data obtained using air as the test fluid [73]. The performance of the flow regime maps was determined using 70 experimental data points (220 < Re < 743, Pr ≈ 0.7, 0.13 < Gr < 1 000), and the flow regime maps could predict 86% of the data within 10% and all the data within 20%.

The flow regime maps in Fig. 17 to Fig. 20 were generated using developing flow and fully developed flow data. The validity/accuracy of these flow regime maps in the laminar flow regime using fully developed data only was determined by comparing Nu/Nu_{SL} of the experimental data and the Nu/Nu_{FC} values in the four flow regime maps, and the results are summarised in Table 12. Because all four flow regime maps could predict almost all the data within 20%, it is confirmed that these flow regime maps can be used as reliable tools to predict the convection flow regime for both developing and fully developed flow in a wide range of tube diameters and Prandtl numbers.

Table 12: Performance of the flow regime maps in Fig. 17 to Fig. 20 using fully developed data only [26].

	Everts and Meyer [26]				Everts and Meyer [26] and literature [28, 65]			
Range	546 ≤ Re ≤ 2 936, 3 ≤ Pr ≤ 6.5, 2.7 ≤ Gz ≤ 45, 137 ≤ Gr ≤ 9.4×10^4, 610 ≤ Gr^* ≤ 1.2×10^6				546 ≤ Re ≤ 2 936, 3 ≤ Pr ≤ 139.5, 2.7 ≤ Gz ≤ 1 241, 137 ≤ Gr ≤ 4.2×10^5, 610 ≤ Gr^* ≤ 7.0×10^6			
	n	±10% [%]	±20% [%]	Ave %	n	±10% [%]	±20% [%]	Ave %
$Ri(x/D)$: Fig. 17	917	73	95	7.1	985	72	94	7.4
Ra/Gz: Fig. 18	917	74	95	7.1	985	72	94	7.3
$Ri^*(x/D)$: Fig. 19	917	85	99	5.3	985	83	98	5.7
Ra^*/Gz: Fig. 20	917	85	99	5.3	985	84	98	5.6

10. Conclusions

The purpose of this chapter was to combine fragmented previous work of the authors to create a new coherent body of work with new perspectives. Specifically, focussing on the heat transfer and pressure drop characteristics of developing and fully developed flow of low Prandtl number fluids in smooth horizontal tubes for forced and mixed convection conditions. The flow regimes that were covered

were laminar (forced and mixed convection), transitional (forced and mixed convection), quasi-turbulent and turbulent.

The boundaries between the flow regimes were defined mathematically, and terminology to define transitional flow characteristics were presented. Three different regions, namely forced convection developing (FCD), mixed convection developing (MCD) and fully developed (FD) exist in the local laminar heat transfer results and nomenclature and correlations to define and quantify the boundaries of these regions were also presented. When the flow is simultaneously hydrodynamically and thermally developing, a longer thermal entrance length is required than when the flow is hydrodynamically fully developed and thermally developing. A coefficient of at least 0.12 (and not 0.05 as suggested in most literature) was therefore suggested for simultaneously hydrodynamically and thermally developing forced convection laminar flow.

The laminar-turbulent transition along the tube length occurs faster with increasing Reynolds number, due to the increased velocity of the fluid. Furthermore, this transition is also influenced by free convection effects. Free convection effects initially disturb the fluctuations inside the test section, causing a slower laminar-turbulent transition compared with forced convection conditions. However, as the free convection effects are increased further, the fluctuations inside the test section are enhanced. The enhanced mixing causes the laminar-turbulent transition along the tube length to occur faster and the magnitude of the Nusselt numbers to increase.

In the transitional flow regime itself, it was found that the Reynolds number at which transition starts is independent of axial position for both developing and fully developed flow and transition occurs at the same moment in time along the whole tube length. However, the end of transition is dependent on axial position when the flow is developing and occurs earlier as the flow approaches fully developed flow. Once the flow is fully developed, the end of transition becomes independent of axial position. Free convection effects affect both the start and end of the transitional flow regime and cause the Reynolds number range of the transitional flow regime to decrease. Correlations to determine the start and end of the transitional flow regime for developing and fully developed flow in mixed convection conditions were therefore presented.

The transitional flow regime across the tube length can be divided into three regions. In the first region, the width of the transitional flow regime decreases significantly with axial position as the thermal boundary layer thickness increases and free convection effects are negligible. In Region 2, the width of the transitional flow regime decreases with axial position, due to the development of the thermal boundary layer and the mass flow rate and temperature fluctuations, as well as with free convection effects. In the fully developed region (Region 3), the width of the transitional flow regime is independent of axial position, but decreases significantly with increasing free convection effects. At high Grashof numbers, free convection effects even cause the transitional flow regime to become negligible when the flow is fully developed and the flow alternates between the laminar and the quasi-turbulent flow regimes.

The boundaries of the different flow regimes are the same for pressure drop and heat transfer, and a relationship between pressure drop and heat transfer exists in all four flow regimes. In the laminar flow regime, this relationship is a function of Grashof number, while it is a function of Reynolds number in the other three flow regimes. Correlations to predict the friction factors as a function of

average Nusselt number, as well as correlations to predict the average Nusselt number for developing and fully developed flow in all flow regimes, were presented.

Finally, a total of six flow regime maps were presented and these flow regime maps are unique for four reasons. Firstly, they contain contour lines that show the Nusselt number enhancements due to the free convection effects. Secondly, they are valid for a wide range of tube diameters and Prandtl numbers. Thirdly, the flow regime maps are developed as a function of temperature difference (Grashof number) and heat flux (modified Grashof number). Finally, four of the six flow regime maps are not only valid for fully developed flow, but also for developing flow. These flow regime maps can be used as reliable tools to predict the convection flow regime for developing and fully developed flow for a wide range of tube diameters and Prandtl numbers.

Overall, it can be concluded that free convection effects significantly affect the thermal entrance length, laminar-turbulent transition along the tube length, as well as the local heat transfer and pressure drop characteristics in the laminar and transitional flow regime. Furthermore, the heat transfer and pressure drop characteristics of developing and fully developed flow are significantly different, especially in the transitional flow regime. The thermal entrance length, heat transfer and pressure drop correlations, as well as the flow regime maps, that were presented in this chapter will not only enable designers to optimise the design of heat exchangers, but also improve the fundamental understanding of mixed convection developing and fully developed flow.

11. Recommendations

The following future work is recommended:

- The definition of the boundary between the quasi-turbulent and turbulent flow regimes can be improved by using experimental data with lower uncertainties (experiments conducted at higher heat fluxes) in the quasi-turbulent and turbulent flow regimes.
- The inflection point in the transitional flow regime is where the trend of the flow characteristics changes. The inflection point was found to be in the middle of the transitional flow regime and was prominent in both the heat transfer and pressure drop results, as well as when the relationship between pressure drop and heat transfer was investigated. The understanding of the heat transfer and pressure drop characteristics in the transitional flow regime can be improved by investigating the physics of the inflection point.
- When the Reynolds number exceeded the critical Reynolds number, four different regions were identified; however, the boundaries and heat transfer characteristics of these regions in the transitional flow regime were not quantified. The reason was that the laminar-turbulent transition along the tube length was significantly affected by fluid velocity as well as free convection effects, and therefore occurred faster with both increasing Reynolds number and Grashof number. This should be further investigated to develop correlations to determine the boundaries of the different regions in the transitional flow regime, as well as to predict the local Nusselt numbers as a function of axial position for transitional flow.
- Experimental data from literature were used to ensure that a wider range of Prandtl number data were available to use for interpretation and the development of correlations. To better investigate the influence of Prandtl numbers on the local heat transfer characteristics of developing and fully developed flow, experiments should be conducted using the same (or modified) experimental set-up, but with different concentrations of ethylene glycol-water

mixtures as the test fluid. The results can then be compared with the low Prandtl number results obtained in this study. This will extend the experimental data base of the heat transfer and pressure drop results in the transitional flow regime. It will also improve the accuracy and extend the ranges of the correlations and flow regime maps that were developed in this chapter.

- For Prandtl numbers less than one, the thermal boundary layer develops faster than the hydrodynamic boundary. It will be valuable to conduct experiments using air ($Pr < 1$) to determine the validity/accuracy of the correlations and flow regime maps developed in this study for Prandtl numbers less than one. If necessary, the correlations and flow regime maps can then be modified to be valid for all Prandtl numbers.
- When the surface roughness of the tube is increased, the velocity and thermal boundary layers will be affected. This will not only affect the thermal entrance length and pressure drop, but also free convection effects and thus the heat transfer coefficients. Because the transitional flow regime is very dependent on free convection effects and developing flow, this will also significantly influence the heat transfer and pressure drop characteristics in the transitional flow regime, as well as the boundaries of the transitional flow regime. In order to investigate the influence of surface roughness on the heat transfer and pressure characteristics in all flow regimes, experiments should be conducted in test sections with different values of relative surface roughness. The results can then be compared with the smooth tube results. Thermal entrance length, heat transfer and pressure drop correlations that account for surface roughness, developing flow and mixed convection conditions can then be developed. This will be of great value to design engineers because corrosion and scaling are common problems in heat exchangers, which not only increase the surface roughness of the tube, but also affect the performance of the heat exchangers.

Nomenclature

A_c	Cross-sectional area ($=\pi D^2/4$)	m^2
C	Coefficient used in correlations	
C_p	Constant-pressure specific heat	J/kg.K
D	Inner diameter	m
f	Friction factor ($=\Delta P \rho D^5 \pi^2/(8\dot{m}L)$)	
f_{cr}	Friction factor at Re_{cr}	
f_{qt}	Friction factor at Re_{qt}	
g	Gravitational acceleration	m/s^2
Gr	Grashof number ($=g\beta(T_S-T_m)D^3/v^2$)	
Gr^*	Modified Grashof number ($=NuGr=g\beta\dot{q}D^4/(kv^2)$)	
Gz	Graetz number ($=RePrD/x$)	
h	Heat transfer coefficient ($=\dot{q}/(T_s-T_m)$)	$W/m^2.°C$
j	Colburn j-factor ($=Nu/(RePr^{1/3})$)	
j_{cr}	Colburn j-factor at Re_{cr}	
j_{qt}	Colburn j-factor at Re_{qt}	
k	Thermal conductivity	W/m.K
L	Length	m
Lt	Thermal entrance length	m
$\dot{m}$	Mass flow rate	kg/s
n	Total	
Nu	Nusselt number ($=hD/k$)	
ΔP	Pressure drop	Pa

Pr	Prandtl number	
$\dot{q}$	Heat flux (=$\dot{m}C_p(T_o-T_i)/(\pi DL)$)	W/m^2
Ra	Rayleigh number (=$GrPr$)	
Ra^*	Modified Rayleigh number (=Gr^*Pr)	
Re	Reynolds number (=$\dot{m}D/\mu A_c$)	
Re'	Transitional flow inflection point	
Re_{cr}	Critical Reynolds number	
Re_{qt}	Start of quasi-turbulent flow regime	
Re_t	Start of turbulent flow regime	
ΔRe	Width of transitional flow regime	
Ri	Richardson number (=Gr/Re^2)	
Ri^*	Modified Richardson number (=Gr^*/Re^2)	
T	Temperature	°C or K
TG_f	Transition gradient in terms of friction factor results	
TG_j	Transition gradient in terms of Colburn j-factor factor results	
x	Distance from inlet	m
z^*	=$\pi/(4Gz)$ as in Eq. (48)	

Greek letters

β	Thermal expansion coefficient	1/K
μ	Dynamic viscosity	kg/m.s
ν	Kinematic viscosity	m^2/s
ρ	Density	kg/m^3

Superscripts

-	Average

Subscripts

b	Bottom/bulk
FC	Forced convection
i	Index/inlet
L	Laminar
QT	Quasi-turbulent
s	Surface
SL	Shah and London [60] Nusselt number correlation
T	Turbulent
t	Top
TG	Transition gradient

Abbreviations (also used as italic subscripts)

FC/MC	forced/mixed convection boundary
FCD	forced convection developing region
FCD/MCD	boundary between FCD and MCD regions
FCD/FD	boundary between FCD and FD regions
FD	fully developed region
MCD	mixed convection developing region
MCD/FD	boundary between MCD and FD regions

References

[1] K.C. Cheng, J.W. Ou, Free convection effects on Graetz problem for large Prandtl number fluids in horizontal tubes with a uniform wall heat flux, in: 5th International Heat Transfer Conference (IHTC-5), Tokyo, Japan, 1974, pp. 159-163.

[2] A.J. Ghajar, J. Kim, Calculation of local inside-wall convective heat-transfer parameters from measurements of local outside-wall temperatures along an electrically heated circular tube, in: M. Kutz (Ed.) Heat-Transfer Calculations, McGraw-Hill, New York, 2006, pp. 23.23-23.27.

[3] A.J. Ghajar, K.F. Madon, Pressure drop measurements in the transition region for a circular tube with three different inlet configurations, Exp. Therm. Fluid Sci., 5(1) (1992) 129-135.

[4] A.J. Ghajar, R.P. Rao, W.L. Cook, C.C. Tang, An experimental study of friction factor in the transition region for single phase flow in mini- and micro-tubes, in: 6th International Conference on Nanochannels, Microchannels, and Minichannels (ICNMM2008), Darmstadt, Germany, 2008, pp. 249-257.

[5] A.J. Ghajar, L.M. Tam, Flow regime map for a horizontal pipe with uniform wall heat flux and three inlet configurations, Exp. Therm. Fluid Sci., 10(3) (1995) 287-297.

[6] A.J. Ghajar, L.M. Tam, Heat transfer measurements and correlations in the transition region for a circular tube with three different inlet configurations, Exp. Therm. Fluid Sci., 8(1) (1994) 79-90.

[7] A.J. Ghajar, L.M. Tam, Laminar-transition-turbulent forced and mixed convective heat transfer correlations for pipe flows with different inlet configurations, in: Winter Annual Meeting of the American Society of Mechanical Engineers, Publ by ASME, New York, United States, 1991, pp. 15-23.

[8] A.J. Ghajar, C.C. Tang, W.L. Cook, Experimental investigation of friction factor in the transition region for water flow in minitubes and microtubes, Heat Transfer Eng, 31(8) (2010) 646-657.

[9] D. Taler, A new heat transfer correlation for transition and turbulent fluid flow in tubes, Int. J. Therm. Sci., 108 (2016) 108-122.

[10] H.K. Tam, L.M. Tam, A.J. Ghajar, Effect of inlet geometries and heating on the entrance and fully-developed friction factors in the laminar and transition regions of a horizontal tube, Exp. Therm. Fluid Sci., 44 (2013) 680-696.

[11] H.K. Tam, L.M. Tam, A.J. Ghajar, C.W. Cheong, Development of a unified flow regime map for a horizontal pipe with the support vector machines, in: 2nd International Symposium on Computational Mechanics (ISCM II), Hong Kong, 2010, pp. 608-613.

[12] H.K. Tam, L.M. Tam, A.J. Ghajar, S.C. Tam, T. Zhang, Experimental investigation of heat transfer, friction factor, and optimal fin geometries for the internally microfin tubes in the transition and turbulent regions, J. Enhanced Heat Transf., 19(5) (2012) 457-476.

[13] L.M. Tam, An experimental investigation of heat transfer and pressure drop in the transition region for a horizontal tube with different inlets and uniform heat flux, PhD thesis, Oklahoma State University, Stillwater, 1995.

[14] L.M. Tam, A.J. Ghajar, The unusual behavior of local heat transfer coefficient in a circular tube with a bell-mouth inlet, Exp. Therm. Fluid Sci., 16(3) (1998) 187-194.

[15] L.M. Tam, A.J. Ghajar, Effect of inlet geometry and heating on the fully developed friction factor in the transition region of a horizontal tube, Exp. Therm. Fluid Sci., 15(1) (1997) 52-64.

[16] L.M. Tam, A.J. Ghajar, Transitional heat transfer in plain horizontal tubes, Heat Transfer Eng, 27(5) (2006) 23-38.

[17] L.M. Tam, A.J. Ghajar, H.K. Tam, S.C. Tam, Development of a flow regime map for a horizontal pipe with the multi-classification Support Vector Machines, in: 2008 ASME Summer Heat Transfer Conference (HT2008), Jacksonville, USA, 2009, pp. 537-547.

[18] L.M. Tam, H.K. Tam, A.J. Ghajar, W.S. Ng, C.K. Wu, The effect of inner surface roughness and heating on friction factor in horizontal mini-tubes, in: 15th International Heat Transfer Conference (IHTC-15), Kyoto, Japan, 2014.

[19] S.M. Abolarin, M. Everts, J.P. Meyer, Heat transfer and pressure drop characteristics of alternating clockwise and counter clockwise twisted tape inserts in the transitional flow regime, Int. J. Heat Mass Transf., (2019) 203-217.

[20] S.M. Abolarin, M. Everts, J.P. Meyer, The influence of peripheral u-cut twisted tapes and ring inserts on the heat transfer and pressure drop characteristics in the transitional flow regime, Int. J. Heat Mass Transf., (2019) 970-984.
[21] J. Dirker, J.P. Meyer, D.V. Garach, Inlet flow effects in micro-channels in the laminar and transitional regimes on single-phase heat transfer coefficients and friction factors, Int. J. Heat Mass Transf., 77 (2014) 612-626.
[22] M. Everts, Single-phase mixed convection of developing and fully developed flow in smooth horizontal circular tubes in the laminar, transitional, quasi-turbulent and turbulent flow regimes, PhD thesis, University of Pretoria, Pretoria, 2017.
[23] M. Everts, J.P. Meyer, Comparison of the heat transfer characteristics of developing and fully developed flow in smooth tubes in the transitional flow regime, in: 12th International Conference on Heat Transfer, Fluid Mechanics and Thermodynamics (HEFAT), Costa del Sol, Spain, 2016.
[24] M. Everts, J.P. Meyer, Heat transfer of developing and fully developed flow in smooth horizontal tubes in the transitional flow regime, Int. J. Heat Mass Transf., 117 (2018) 1331-1351.
[25] M. Everts, J.P. Meyer, Relationship between pressure drop and heat transfer of developing and fully developed flow in smooth horizontal circular tubes in the laminar, transitional, quasi-turbulent and turbulent flow regimes, Int. J. Heat Mass Transf., 117 (2018) 1231-1250.
[26] M. Everts, J.P. Meyer, Flow regime maps for smooth horizontal tubes at a constant heat flux, Int. J. Heat Mass Transf., 117 (2018) 1274-1290.
[27] J.P. Meyer, Heat transfer in tubes in the transitional flow regime, in: 15th International Heat Transfer Conference (IHTC-15), Kyoto, Japan, 2014.
[28] J.P. Meyer, S.M. Abolarin, Heat transfer and pressure drop in the transitional flow regime for a smooth circular tube with twisted tape inserts and a square-edged inlet, Int. J. Heat Mass Transf., 117 (2018) 11-29.
[29] J.P. Meyer, A.I. Bashir, M. Everts, Single-phase mixed convective heat transfer and pressure drop in the laminar and transitional flow regimes in smooth inclined tubes heated at a constant heat flux, Exp. Therm. Fluid Sci., (2019).
[30] J.P. Meyer, A. Du Preez, Heat transfer and pressure drop characteristics of water in the transitional flow regime of horizontal smooth tubes at constant wall temperature, in: 14th International Heat Transfer Conference (IHTC-14), Washington DC, United Stares, 2010, pp. 437-444.
[31] J.P. Meyer, M. Everts, Single-phase mixed convection of developing and fully developed flow in smooth horizontal circular tubes in the laminar and transitional flow regimes, Int. J. Heat Mass Transf., 117 (2018) 1251-1273.
[32] J.P. Meyer, M. Everts, N. Coetzee, K. Grote, M. Steyn, Heat transfer characteristics of quasi-turbulent and turbulent flow in smooth circular tubes, International Communications in Heat and Mass Transfer, 105 (2019) 84-106.
[33] J.P. Meyer, M. Everts, A.T.C. Hall, F.A. Mulock Houwer, M. Joubert, L.M.J. Pallent, E.S. Vause, Inlet tube spacing and protrusion effects on multiple circular tubes in the laminar, transitional and turbulent flow regimes, Int. J. Heat Mass Transf., 118 (2018) 257-274.
[34] J.P. Meyer, L. Liebenberg, J.A. Olivier, Measurement and evaluation of single-phase heat transfer and pressure drop inside enhanced tubes for transition flow, 1280-RP, 2008.
[35] J.P. Meyer, L. Liebenberg, J.A. Olivier, Single-phase heat transfer and pressure drop of water cooled inside horizontal smooth tubes in the transitional flow regime, in: 14th International Heat Transfer Conference, Washington DC, United Stares, 2010, pp. 429-436.
[36] J.P. Meyer, T.J. McKrell, K. Grote, The influence of multi-walled carbon nanotubes on single-phase heat transfer and pressure drop characteristics in the transitional flow regime of smooth tubes, Int. J. Heat Mass Transf., 58(1-2) (2013) 597-609.
[37] J.P. Meyer, J.A. Olivier, Heat transfer and pressure drop characteristics of smooth horizontal tubes in the transitional flow regime, Heat Transfer Eng, 35(14-15) (2014) 1246-1253.

[38] J.P. Meyer, J.A. Olivier, Transitional flow inside enhanced tubes for fully developed and developing flow with different types of inlet disturbances: Part II - Heat transfer, Int. J. Heat Mass Transf., 54(7-8) (2011) 1598-1607.
[39] J.P. Meyer, J.A. Olivier, Transitional flow inside enhanced tubes for fully developed and developing flow with different types of inlet disturbances: Part I - Adiabatic pressure drops, Int. J. Heat Mass Transf., 54(7-8) (2011) 1587-1597.
[40] J.P. Meyer, J.A. Olivier, Heat transfer in the transitional flow regime, in: A. Ahsan (Ed.) Evopration, Condensation and Heat Transfer, InTech, 2011, pp. 245-260.
[41] D.D. Ndenguma, J. Dirker, J.P. Meyer, Transitional flow regime heat transfer and pressure drop in an annulus with non-uniform wall temperatures, Int. J. Heat Mass Transf., 108 (2017) 2239-2252.
[42] D.D. Ndenguma, J. Dirker, J.P. Meyer, Heat transfer and pressure drop in annuli with approximately uniform internal wall temperatures in the transitional flow regime, Int. J. Heat Mass Transf., 111 (2017) 429-441.
[43] J.A. Olivier, J.P. Meyer, Single-phase heat transfer and pressure drop of the cooling of water inside smooth tubes for transitional flow with different inlet geometries (RP-1280), HVAC R Res, 16(4) (2010) 471-496.
[44] J.P. Abraham, E.M. Sparrow, J.C.K. Tong, Breakdown of laminar pipe flow into transitional intermittency and subsequent attainment of fully developed intermittent or turbulent flow, Numer Heat Transfer Part B Fundam, 54(2) (2008) 103-115.
[45] J.P. Abraham, E.M. Sparrow, J.M. Gorman, Y. Zhao, W.J. Minkowycz, Application of an intermittency model for laminar, transitional, and turbulent internal flows, J Fluids Eng Trans ASME, 141(7) (2019).
[46] J.P. Abraham, E.M. Sparrow, W.J. Minkowycz, Internal-flow Nusselt numbers for the low-Reynolds-number end of the laminar-to-turbulent transition regime, Int. J. Heat Mass Transf., 54(1-3) (2011) 584-588.
[47] J.P. Abraham, E.M. Sparrow, J.C.K. Tong, Heat transfer in all pipe flow regimes: laminar, transitional/intermittent, and turbulent, Int. J. Heat Mass Transf., 52(3-4) (2009) 557-563.
[48] T. Wei, J. Abraham, Heat transfer regimes in fully developed circular tube flows, a map of flow regimes, International Communications in Heat and Mass Transfer, 104 (2019) 147-152.
[49] V. Gnielinski, On heat transfer in tubes, Int. J. Heat Mass Transf., 63 (2013) 134-140.
[50] B.S. Gill, Relationship between pressure drop and heat transfer coefficient, Hydrocarbon Processing, 79(8) (2000).
[51] Y.A. Cengel, A.J. Ghajar, Heat and Mass Transfer: Fundamentals and Applications, 5th ed., McGraw-Hill, 2015.
[52] N.T. Obot, Smooth tube friction and heat transfer in laminar and transitional flow, International Communications in Heat and Mass Transfer, 19(3) (1992) 299-310.
[53] R. Allen, E. Eckert, Friction and heat-transfer measurements to turbulent pipe flow of water (Pr = 7 and 8) at uniform wall heat flux, Journal of Heat Transfer, 86(3) (1964) 301-310.
[54] F. Durst, S. Ray, B. Ünsal, O.A. Bayoumi, The development lengths of laminar pipe and channel flows, J Fluids Eng Trans ASME, 127(6) (2005) 1154-1160.
[55] Y. Mori, K. Futagami, S. Tokuda, M. Nakamura, Forced convective heat transfer in uniformly heated horizontal tubes, (1st report) Experimental study on the effect of buoyancy, Int. J. Heat Mass Transf., 9 (1966) 453-463.
[56] H.A. Mohammed, Y.K. Salman, The effects of different entrance sections lengths and heating on free and forced convective heat transfer inside a horizontal circular tube, International Communications in Heat and Mass Transfer, 37 (2007) 769-784.
[57] M. Everts, Heat transfer and pressure drop of developing flow in smooth tubes in the transitional flow regime, Master's dissertation, University of Pretoria, Pretoria, 2014.
[58] A. Faghri, Y. Zhang, J.R. Howell, Advanced Heat and Mass Transfer, Global Digital Press, Columbia, 2010.
[59] J.C. Han, Analytical Heat Transfer, CRC Press, Boca Raton, 2016.

[60] R.K. Shah, A.L. London, Laminar Flow Forced Convection in Ducts, Academic Press, New York, 1978.
[61] P.S. Ghoshdastidar, Heat Transfer, 2nd ed., Oxford University Press, New Delhi, 2012.
[62] R. Siegel, E.M. Sparrow, T.M. Hallman, Steady laminar heat transfer in a circular tube with a prescribed wall heat flux, Applied Scientific Research, 7 (1958).
[63] E.K. Kalinin, S.A. Yarkho, Flow pulsations and heat transfer in the transition region between the laminar and turbulent flow regimes in a tube, International Chemical Engineering, 6(4) (1966) 571-574.
[64] S.W. Hong, S.M. Morcos, A.E. Bergles, Analytical and experimental results for combined forced and free laminar convection in horizontal tubes, in: 5th International Heat Transfer Conference (IHTC-5), Tokyo, 1974, pp. 154-158.
[65] D.T. Strickland, Heat transfer measurements in the transition region for a horizontal circular tube with a square-edged entrance, Master's dissertation, Oklahoma State University, Stillwater, 1990.
[66] J. Chen, Heat transfer in high laminar, transition and lower turbulent flow regimes for square-edged contraction entrance in a circular tube, PhD thesis, Oklahoma State University, Oklahoma, 1988.
[67] J.P. Meyer, C.C. Tang, Convective Heat Transfer of Nanofluids in Tubes, in: S.M. Sohel Murshed, C.A. Nieto de Castro (Eds.) Nanofluids: Synthesis, Properties and Applications, Nova Science Publishers, New York, 2014, pp. 155-192.
[68] W.L. Friend, A.B. Metzner, Turbulent heat transfer inside tubes and the analogy among heat, mass, and momentum transfer, AIChE Journal, 4(4) (1958) 393-402.
[69] V. Gnielinski, New equations for heat and mass-transfer in turbulent pipe and channel flow, International Chemical Engineering, 16(2) (1976) 359-368.
[70] F.M. White, Fluid Mechanics, 6th ed., McGraw-Hill, Singapore, 2009.
[71] S.W. Churchill, R. Usagi, A general expression for the correlation of rates of transfer and other phenomena, AIChE Journal, 18(6) (1972) 1121-1128.
[72] B. Metais, E. Eckert, Forced, mixed, and free convection regimes, Journal of Heat Transfer, 86(2) (1964) 295-296.
[73] S. McComas, E. Eckert, Combined free and forced convection in a horizontal circular tube, Journal of Heat Transfer, 88(2) (1966) 147-152.